Neutron Star Structure, Evolution and Measurements

J. M. Lattimer

Department of Physics & Astronomy

STONY BROOK UNIVERSITY

U.S. DEPARTMENT OF ENERGY

Office of Science

Special Nuclear Physics Lecture Series
Yonsei University, Seoul, Korea, 26-30 June 2023

Outline

- Neutron Star Structure
- Dense Matter Equation of State
- Nuclear Experimental Constraints
- Formation and Evolution of Neutron Stars
- Observational Constraints

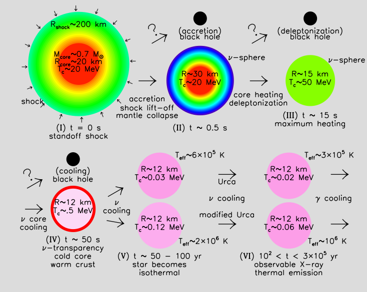

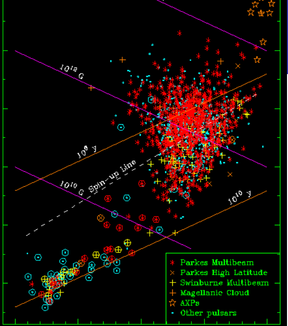

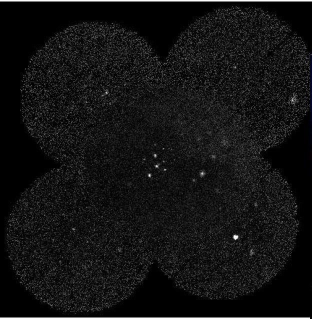

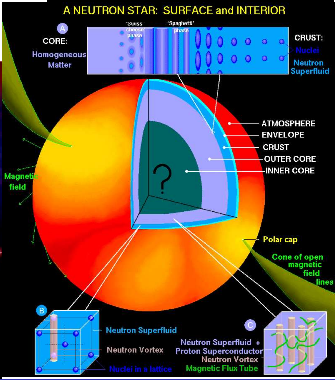

Dany Page, UNAM

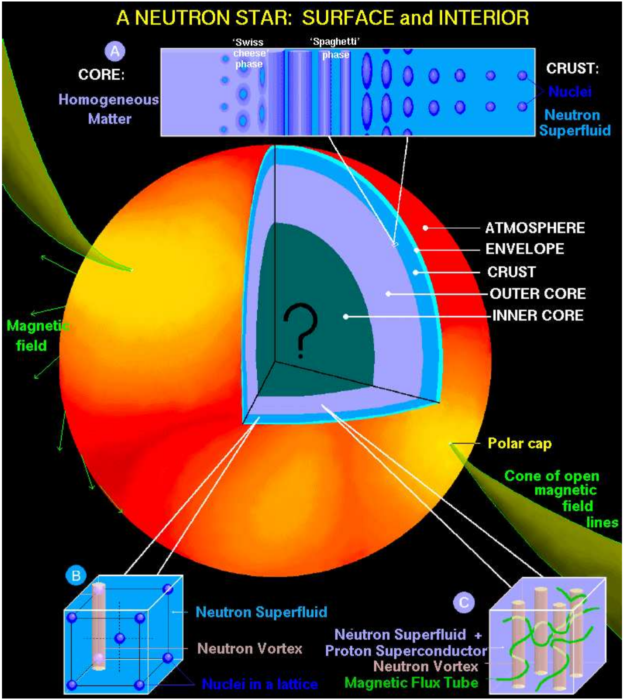

Amazing Facts About Neutron Stars

- Densest objects this side of an event horizon: 10^{15} g cm^{-3}
  Four teaspoons on Earth would weigh as much as the Moon.
- Largest surface gravity: 10^{14} cm s^{-2}
  This is 100 billion times the Earth's gravity.
- Fastest spinning objects known: $\nu = 716$ Hz
  Spin rate measured for PSR J1748-2446ad,
  in the globular cluster Terzan 5, 9 kpc distant.
  33 pulsars have been found in this cluster.
  If $R_{eq} \sim 15$ km, $v_{eq} \sim c/4$.

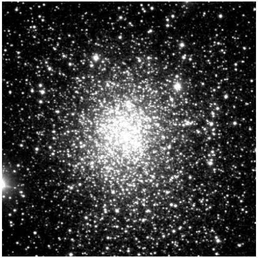

- Largest known magnetic field: $B = 10^{15}$ G
- Highest temperature superconductor: $T_c = 10$ billion K
  The highest known superconductor on the Earth is mercury thallium barium calcium copper oxide ($Hg_{12}T_{l3}Ba_{30}Ca_{30}Cu_{45}O_{125}$), at 138 K.
- Highest temperature, at birth, anywhere in the Universe since the Big Bang: $T = 700$ billion K
- PSR B1508+55 has fastest measured stellar velocity in the Galaxy: 1083 km/s $= c/300$
- The only place in the universe except for the Big Bang where neutrinos become *trapped*.

Neutron Stars: History

1920 Rutherford predicts the neutron
1931 Landau *anticipates* single-nucleus stars but not neutron stars
1932 Chadwick discovers the neutron.
1934 W. Baade and F. Zwicky predict existence of neutron stars as end products of supernovae.
1939 Oppenheimer and Volkoff predict upper mass limit of neutron star.
1964 Hoyle, Narlikar and Wheeler predict neutron stars rapidly rotate.
1965 Hewish and Okoye discover an intense radio source in the Crab nebula.
1966 Colgate and White perform simulations of supernovae leading to neutron stars.
1967 C. Schisler discovers a dozen pulsing radio sources, including the Crab pulsar, using secret military radar in Alaska. X-1.
1967 Hewish, Bell, Pilkington, Scott and Collins discover "first" PSR 1919+21, Aug 6.
1968 The Crab Nebula pulsar is discovered, found to be slowing down (ruling out binary and vibrational models), and clinched the connection to supernovae.
1968 The term "pulsar" first appears in print, in the *Daily Telegraph*.

1969 "Glitches" observed; evidence for superfluidity in neutron star crust.
1971 Accretion powered X-ray pulsar discovered by Uhuru (*not* the Lt.).
1974 Hewish awarded Nobel Prize (but Bell and Okoye were not).
1974 Binary pulsar PSR 1913+16 discovered by Hulse and Taylor., orbital decay due to GR gravitational radiation
1979 Chart recording of PSR 1919+21 used as album cover for *Unknown Pleasures* by Joy Division (#19/100 greatest British album).
1982 First millisecond pulsar, PSR B1937+21, discovered by Backer et al. at Arecibo.
1992 Discovery of first extra-solar planets orbiting PSR B1257+12 by Wolszczan and Frail.
1993 Hulse and Taylor receive Nobel Prize
1998 Kouveletiou et al. discover first magnetar
2004 SGR 1806-20 flares: largest burst of energy seen in Galaxy since SN 1604, brighter than full moon in γ rays, more energy emitted than Sun in 100,000 years.

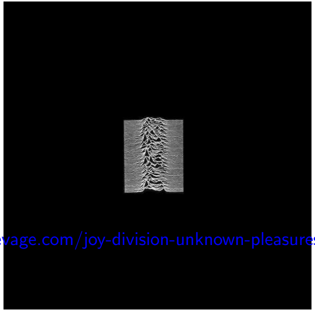

sleevage.com/joy-division-unknown-pleasures/

2004 Hessels et al. discover PSR J1748-2446ad; fastest rotation rate, 716 Hz.
2005 Hessels et al. discover PSR J0737-3039, first two-pulsar binary
2013 Antoniadis et al. find most-massive PSR J0348+0432, 2.01 $M_\odot$
2013 Stairs et al. find first pulsar in triple system

Important Questions

- How Does the Structure of Neutron Stars Depend On the Nucleon-Nucleon Interaction?
  - The Neutron Star Maximum Mass and Causality
  - The Neutron Star Radius and the Nuclear Symmetry Energy
  - Does Exotic Matter (Hyperons, Kaons/Pions, Deconfined Quarks) Exist in Neutron Star Interiors?
- How Do Nuclear Experiments Constrain the Nuclear Symmetry Energy and Neutron Star Radii?
  - Binding Energies
  - Heavy ion Collisions
  - Neutron Skin Thicknesses
  - Dipole Polarizabilities
  - Giant (and Pygmy) Dipole Resonances
  - Pure Neutron Matter
- What Astrophysical Constraints Exist?
  - Nuclear Mass Measurements
  - Photospheric Radius Expansion Bursts
  - Thermal Emission from Isolated and Quiescent Binary Sources
  - Pulse Modeling of X-ray Bursts, QPOs, etc.

Neutron Star Structure

Tolman-Oppenheimer-Volkov equations

$$\frac{dP}{dr} = -\frac{G}{c^2}\frac{(m + 4\pi p r^3/c^2)(\varepsilon + P)}{r(r - 2Gm/c^2)}$$

$$\frac{dm}{dr} = 4\pi\frac{\varepsilon}{c^2}r^2$$

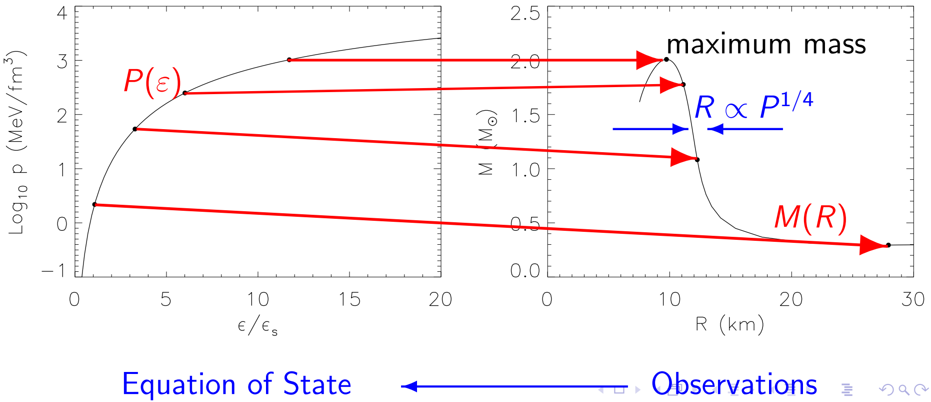

Mass-Radius Diagram and Theoretical Constraints

GR:
$R > 2GM/c^2$

$P < \infty$:
$R > (9/4)GM/c^2$

causality:
$R \gtrsim 2.9GM/c^2$

— normal NS
— SQS

— $R_\infty = \frac{R}{\sqrt{1-2GM/Rc^2}}$

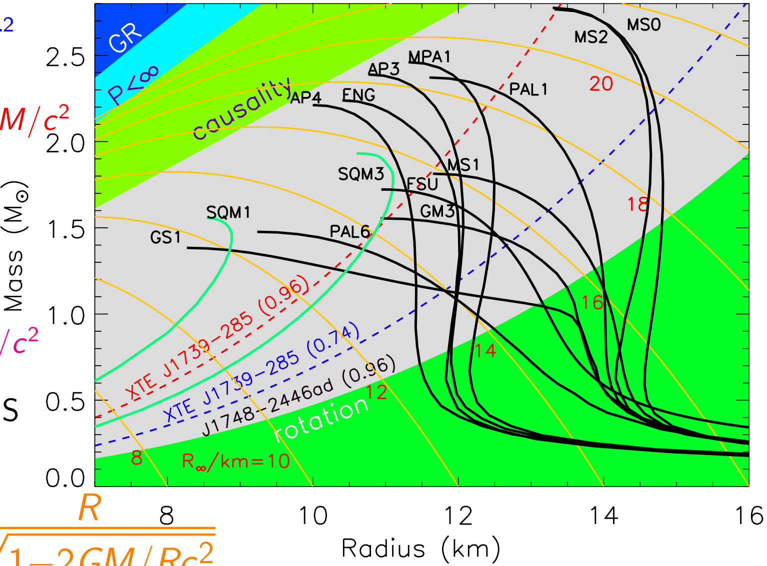

The Radius – Pressure Correlation

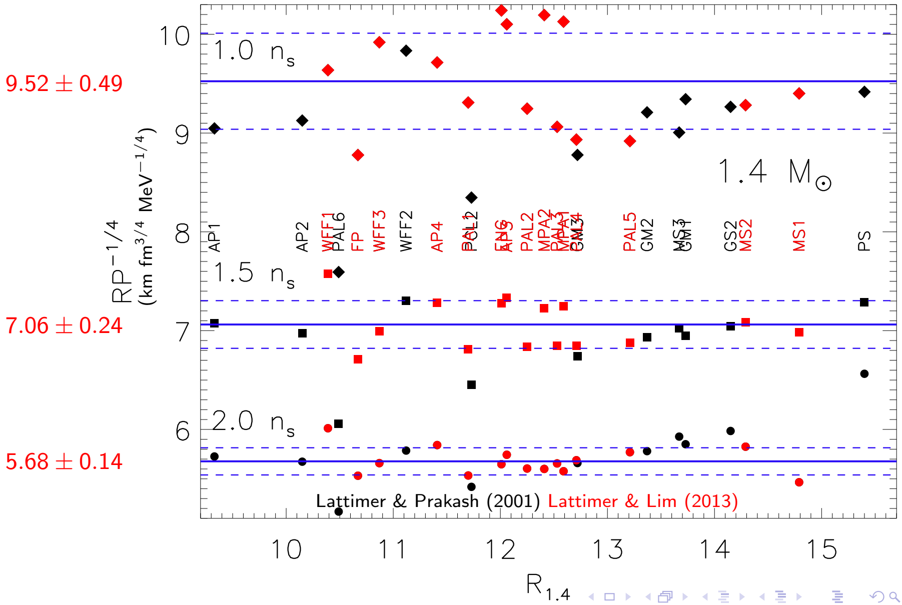

Neutron Star Structure

Newtonian Gravity:

$$\frac{dP}{dr} = -\frac{Gm\rho}{r^2}; \qquad \frac{dm}{dr} = 4\pi\rho r^2; \qquad \rho c^2 = \varepsilon$$

Newtonian Polytrope:

$$P = K\rho^\gamma; \qquad M \propto K^{1/(2-\gamma)} R^{(4-3\gamma)/(2-\gamma)}$$

$$\rho < \rho_s: \ \gamma \simeq \frac{4}{3}; \qquad \rho > \rho_s: \ \gamma \simeq 2$$

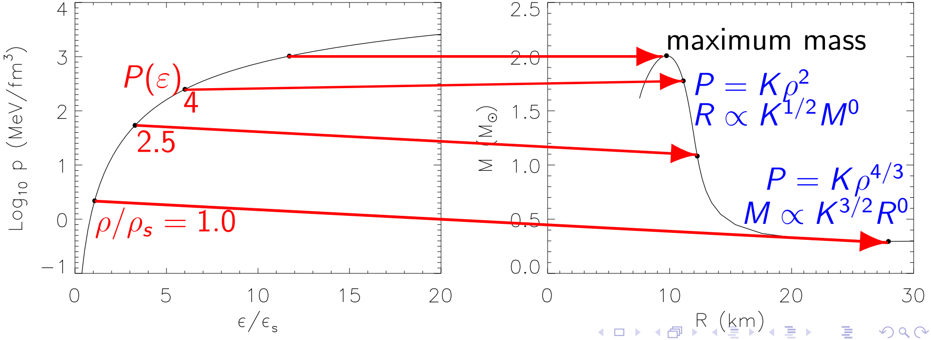

Extremal Properties of Neutron Stars

- The most compact and massive configurations occur when the low-density equation of state is "soft" and the high-density equation of state is "stiff" (Koranda, Stergioulas & Friedman 1997).

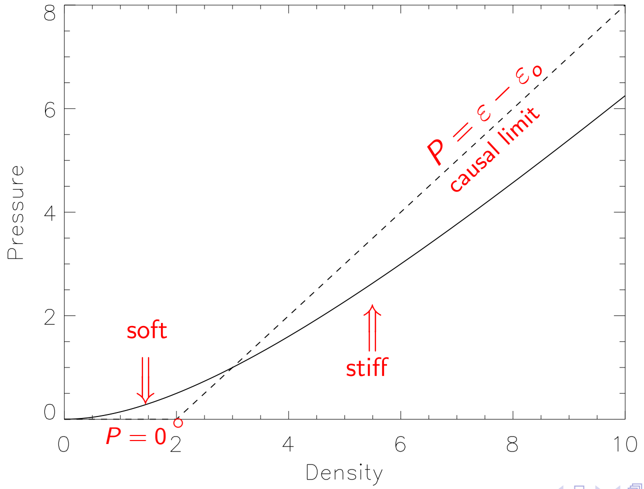

ε_o is the only EOS parameter

The TOV solutions scale with ε_o

$w = \varepsilon/\varepsilon_o$
$y = P/\varepsilon_o = w - 1$
$x = r\sqrt{G\varepsilon_o}/c^2$
$z = m\sqrt{G^3\varepsilon_o}/c^2$

Extremal Properties of Neutron Stars

The maximum mass configuration is achieved when
$x_R = 0.2404$, $w_c = 3.034$, $y_c = 2.034$, $z_R = 0.08513$.

A useful reference density is the nuclear saturation density (interior density of normal nuclei):
$\rho_s = 2.7 \times 10^{14}$ g cm^{-3}, $n_s = 0.16$ baryons fm^{-3}, $\varepsilon_s = 150$ MeV fm^{-3}

- $M_{\rm max} = 4.1\ (\varepsilon_s/\varepsilon_o)^{1/2} M_\odot$ (Rhoades & Ruffini 1974)
- $M_{B,\rm max} = 5.41\ (m_B c^2/\mu_o)(\varepsilon_s/\varepsilon_o)^{1/2} M_\odot$
- $R_{\rm min} = 2.82\ GM/c^2 = 4.3\ (M/M_\odot)\ {\rm km}$
- $\mu_{b,\rm max} = 2.09$ GeV
- $\varepsilon_{c,\rm max} = 3.034\ \varepsilon_o \simeq 51\ (M_\odot/M_{\rm largest})^2\ \varepsilon_s$
- $P_{c,\rm max} = 2.034\ \varepsilon_o \simeq 34\ (M_\odot/M_{\rm largest})^2\ \varepsilon_s$
- $n_{B,\rm max} \simeq 38\ (M_\odot/M_{\rm largest})^2\ n_s$
- $\mathrm{BE}_{\rm max} = 0.34\ M$
- $P_{\rm spin,min} = 0.74\ (M_\odot/M_{\rm sph})^{1/2}(R_{\rm sph}/10\ {\rm km})^{3/2}\ {\rm ms} = 0.20\ (M_{\rm sph,max}/M_\odot)\ {\rm ms}$

Maximum Energy Density in Neutron Stars

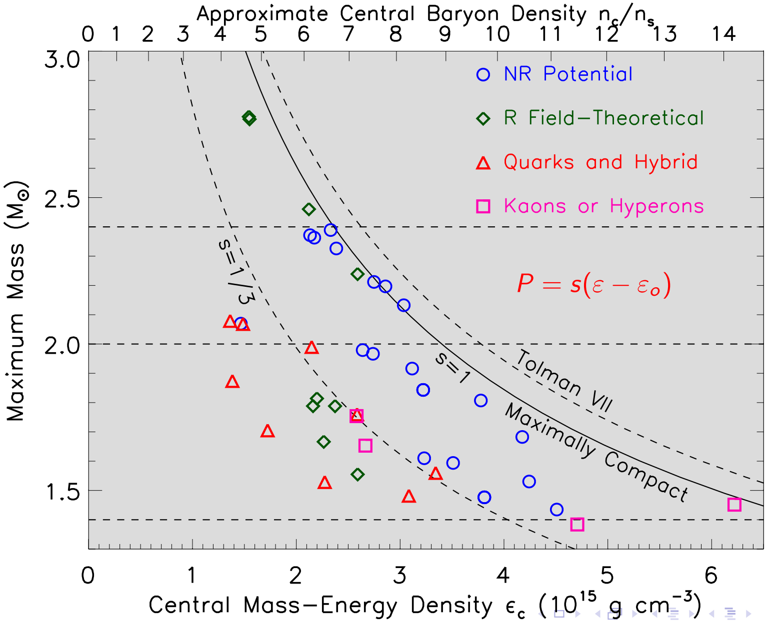

Causality + GR Limits and the Maximum Mass

A lower limit to the maximum mass sets a lower limit to the radius for a given mass.

Similarly, a precise (M, R) measurement sets an upper limit to the maximum mass.

$1.4 M_\odot$ stars must have $R > 8.15 M_\odot$.

$1.4 M_\odot$ strange quark matter stars (and likely hybrid quark/hadron stars) must have $R > 11$ km.

$M - R$ curves for maximally compact EOS

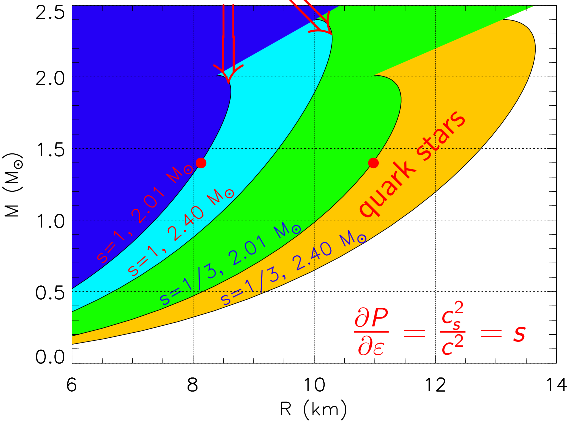

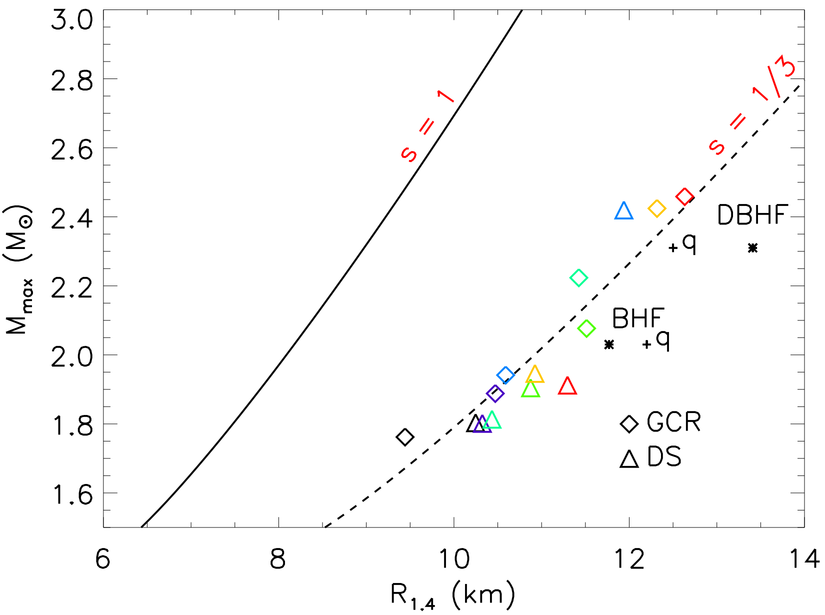
3.0
2.8
2.6
2.4
2.2
2.0
1.8
1.6
6
8
10
12
14
M_{max} ($M_\odot$)
$R_{1.4}$ (km)
s = 1
s = 1/3
DBHF
q
BHF
q
GCR
DS

Spherically Symmetric General Relativity

Static metric:

$$ds^2 = e^{\lambda(r)}dr^2 + r^2\left(d\theta^2 + \sin^2\theta d\phi^2\right) - e^{\nu(r)}dt^2$$

Einstein's equations:

$$\begin{aligned} 8\pi\varepsilon(r)Gr^2/c^4 &= 1 - e^{-\lambda(r)} + re^{-\lambda(r)}\lambda'(r), \\ 8\pi P(r)Gr^2/c^4 &= e^{-\lambda(r)} - 1 + re^{-\lambda(r)}\nu'(r), \\ P'(r) &= -\frac{P(r)+\varepsilon(r)}{2}\nu'(r). \end{aligned}$$

Mass: $m(r)c^2 = 4\pi\int_0^r \varepsilon(r')r'^2dr', \qquad e^{-\lambda(r)} = 1 - 2Gm(r)/(rc^2)$

Boundaries:

$r = 0 \qquad m(0) = P'(0) = \varepsilon'(0) = 0,$

$r = R \qquad m(R) = M, \quad P(R) = 0, \quad e^{\nu(R)} = e^{-\lambda(R)} = 1 - 2GM/(Rc^2)$

Thermodynamics:

$$\begin{aligned} \frac{dn}{n} &= \frac{d\varepsilon}{\epsilon + P} = -\frac{d\varepsilon}{dP}\frac{d\nu}{2}, \quad \mu = \frac{d\varepsilon}{dn}, \quad \frac{\varepsilon}{n} = m_bc^2 + e, \quad \frac{P}{n^2} = \frac{de}{dn} \\ m_bc^2n(r) &= (\varepsilon(r) + P(r))e^{(\nu(r)-\nu(R))/2} - n(R)e(R) \\ N &= \int_0^R 4\pi r^2 e^{\lambda(r)/2}n(r)dr; \qquad \mathrm{BE} = (Nm_b - M)c^2 \end{aligned}$$

Neutron Star Structure

Tolman-Oppenheimer-Volkov equations of relativistic hydrostatic equilibrium:

$$\frac{dP}{dr} = -\frac{G}{c^2}\frac{(m+4\pi r^3 P/c^2)(\varepsilon + P)}{r(r-2Gm/c^2)}$$
$$\frac{dm}{dr} = 4\pi\frac{\varepsilon}{c^2}r^2$$

P is pressure, ε is mass-energy density
Useful analytic solutions exist:

- Uniform density $\varepsilon =$ constant
- Tolman VII $\varepsilon = \varepsilon_c[1-(r/R)^2]$
- Buchdahl $\varepsilon = \sqrt{PP_*} - 5P$

Uniform Density Fluid

$$
\begin{aligned}
m(r) &= \frac{4\pi}{3}\frac{\varepsilon}{c^2}r^3 = Mx^{3/2}, \qquad x \equiv \left(\frac{r}{R}\right)^2, \qquad \beta \equiv \frac{GM}{Rc^2} \\
e^{-\lambda(r)} &= 1 - 2\beta x, \\
e^{\nu(r)} &= \left[\frac{3}{2}\sqrt{1-2\beta} - \frac{1}{2}\sqrt{1-2\beta x}\right]^2, \\
P(r) &= \varepsilon\left[\frac{\sqrt{1-2\beta x} - \sqrt{1-2\beta}}{3\sqrt{1-2\beta} - \sqrt{1-2\beta x}}\right], \\
\varepsilon(r) &= \mathrm{constant}; \qquad n(r) = \mathrm{constant} \\
\frac{\mathrm{BE}}{Mc^2} &= \frac{3}{4\beta}\left(\frac{\sin^{-1}\sqrt{2\beta}}{\sqrt{2\beta}} - \sqrt{1-2\beta}\right) \simeq \frac{3\beta}{5} + \frac{9}{14}\beta^2 + \cdots, \\
c_s^2 &= \infty
\end{aligned}
$$

$$
P_c < \infty \Longrightarrow \beta < 4/9
$$

$$
P_c < \varepsilon \Longrightarrow \beta < 3/8
$$

Tolman VII

$$
\begin{aligned}
\varepsilon(r) &= \varepsilon_c\left[1-(r/R)^2\right] \equiv \varepsilon_c[1-x] \\
e^{-\lambda(r)} &= 1-\beta x(5-3x) \\
e^{\nu(r)} &= (1-5\beta/3)\cos^2\phi, \\
P(r) &= \frac{c^2}{4\pi G R^2}\left[\sqrt{3\beta e^{-\lambda(r)}}\tan\phi(r)-\frac{\beta}{2}(5-3x)\right], \\
n(r) &= \frac{\varepsilon(r)+p(r)}{m_b c^2}\frac{\cos\phi(r)}{\cos\phi_1} \\
\phi(r) &= \frac{w_1-w(r)}{2}+\phi_1, \qquad \phi_1=\phi(x=1)=\tan^{-1}\sqrt{\frac{\beta}{3(1-2\beta)}}, \\
w(r) &= \ln\left[x-\frac{5}{6}+\sqrt{\frac{e^{-\lambda(r)}}{3\beta}}\right], \quad w_1=w(x=1)=\ln\left[\frac{1}{6}+\sqrt{\frac{1-2\beta}{3\beta}}\right].
\end{aligned}
$$

$$
(P/\varepsilon)_c=\frac{2\tan\phi_c}{15}\sqrt{\frac{3}{\beta}-\frac{1}{3}}, \qquad c_{s,c}^2=\tan\phi_c\left(\frac{1}{5}\tan\phi_c+\sqrt{\frac{\beta}{3}}\right)
$$

$$
\frac{\mathrm{BE}}{Mc^2}\simeq\frac{11}{21}\beta+\frac{7187}{18018}\beta^2+\cdots
$$

$$
P, c_s^2<\infty \Longrightarrow \phi_c<\pi/2 \Longrightarrow \beta<0.3862, \qquad c_s^2<1 \Longrightarrow \beta<0.2698.
$$

Buchdahl's Solution: Relativistic n=1 Polytrope

$$\varepsilon = \sqrt{P_* P} - 5P$$

$$\begin{aligned}
e^{\nu(r)} &= (1-2\beta)(1-\beta-u(r))(1-\beta+u(r))^{-1}, \\
e^{\lambda(r)} &= (1-2\beta)(1-\beta+u(r))(1-\beta-u(r))^{-1}(1-\beta+\beta\cos Ar')^{-2}, \\
8\pi P(r) &= A^2 u(r)^2 (1-2\beta)(1-\beta+u(r))^{-2}, \\
8\pi\varepsilon(r) &= 2A^2 u(r)(1-2\beta)(1-\beta-3u(r)/2)(1-\beta+u(r))^{-2}, \\
n(r) m_b c^2 &= \sqrt{p_* p(r)}\left(1-4\sqrt{\frac{p(r)}{p_*}}\right)^{3/2}, \qquad c_s^2(r) = \left(\frac{1}{2}\sqrt{\frac{p_*}{p(r)}}-5\right)^{-1} \\
u(r) &= \frac{\beta}{Ar'}\sin Ar' = (1-\beta)\left(\frac{1}{2}\sqrt{\frac{P_*}{P(r)}}-1\right)^{-1}, \\
r' &= r(1-2\beta)(1-\beta+u(r))^{-1}, \\
A^2 &= 2\pi P_*(1-2\beta)^{-1}, \qquad R = (1-\beta)\sqrt{\frac{\pi c^2}{2GP_*(1-2\beta)}}.
\end{aligned}$$

$$P_c = \frac{P_*}{4}\beta^2, \qquad \varepsilon_c = \frac{P_*}{2}\beta(1-\frac{5}{2}\beta), \qquad n_c m_b c^2 = \frac{P_*}{2}\beta(1-2\beta)^{3/2}$$

$$\mathrm{BE}/(Mc^2) = (1-3/2\beta)(1-2\beta)^{-1/2}(1-\beta)^{-1} \simeq \beta/2 + \beta^2/2 + \cdots$$

$$c_s^2 < \infty \Longrightarrow \beta < 1/5, \qquad c_s^2 < 1 \Longrightarrow \beta < 1/6.$$

Tolman IV Variation: A Self-Bound Star (Quark Star)

$$
\begin{aligned}
e^{\nu(r)} &= \frac{\left[1-\beta\left(\frac{5}{2}-\frac{1}{2}x\right)\right]^2}{(1-2\beta)}, \\
e^{\lambda(r)} &= \frac{\left[1-\beta\left(\frac{5}{2}-\frac{3}{5}x\right)\right]^{2/3}}{\left[1-\beta\left(\frac{5}{2}-\frac{3}{2}x\right)\right]^{2/3}-2(1-\beta)^{2/3}\beta x}, \\
4\pi\frac{G}{c^2}pR^2 &= \frac{\beta}{1-\beta\left(\frac{5}{2}-\frac{1}{2}x\right)}\left[1-(1-\beta)^{2/3}\frac{1-\frac{5}{2}\beta(1-x)}{\left[1-\beta\left(\frac{5}{2}-\frac{3}{2}x\right)\right]^{2/3}}\right], \\
4\pi\frac{G}{c^2}\varepsilon R^2 &= \frac{3(1-\beta)^{2/3}\beta\left[1-\beta(\frac{5}{2}-\frac{5}{6}x)\right]}{\left[1-\beta\left(\frac{5}{2}-\frac{3}{2}x\right)\right]^{5/3}}, \quad m=\frac{(1-\beta)^{2/3}Mx^{3/2}}{\left[1-\beta\left(\frac{5}{2}-\frac{3}{2}x\right)\right]^{2/3}} \\
c_s^2 &= \frac{(2-5\beta+3\beta x)}{5(2-5\beta+\beta x)^3}\left[\frac{(2-5\beta+3\beta x)^{5/3}}{2^{2/3}(1-\beta)^{2/3}}+(2-5\beta)^2-5\beta^2 x\right], \\
\frac{\varepsilon_{surf}}{\varepsilon_c} &= \left(1-\frac{5}{3}\beta\right)\left(1-\frac{5}{2}\beta\right)^{2/3}(1-\beta)^{-5/3}.
\end{aligned}
$$

$$
0.30 < c_{s,c}^2 < 0.44, \qquad 0.265 < \frac{\varepsilon_{surf}}{\varepsilon_c} < 1
$$

Roche Model for Rotation (Shapiro & Teukolsky 1983)

$$\rho^{-1}\nabla P = \nabla\mu = -\nabla(\Phi_G + \Phi_c)$$

$$\Phi_G \simeq -\frac{GM}{r}, \; \Phi_c = -\frac{1}{2}\Omega^2 r^2 \sin^2\theta$$

Bernoulli integral:
$H = \mu + \Phi_G + \Phi_c = -GM/R$
$\mu = \int_0^P \rho^{-1} dP = \mu_n - \mu_{n0}$

Evaluate at equator:

$$\frac{\Omega^2 R_{eq}^3}{2GM} = \frac{R_{eq}}{R} - 1$$

Also true in GR. Mass-shedding limit:
$\Omega_{shed}^2 = GM/R_{eq}^3, \quad R_{eq}/R = \frac{3}{2}$
GR: Cook, Shapiro & Teukolsky (1994):
1.43–1.51

$$\Omega_{shed} = \left(\frac{2}{3}\right)^{3/2}\sqrt{\frac{GM}{R^3}}$$

$$\frac{P_{shed}}{\mathrm{ms}} \simeq 1.00\left(\frac{R}{10\ \mathrm{km}}\right)^{3/2}\left(\frac{\mathrm{M}_\odot}{M}\right)^{1/2}$$

GR (Haensel et al. 2009): $0.92 \pm 3\%$

Shape: $$\frac{\Omega^2 R^3 \sin^2\theta}{2GM} = \frac{R}{R} - 1$$

$$\frac{R}{R(\theta)} = \frac{1}{3} + \frac{2}{3}\cos\left(\frac{1}{3}\cos^{-1}\left[1 - 2\left(\frac{\Omega\sin\theta}{\Omega_{shed}}\right)^2\right]\right)$$

$\Omega \longrightarrow \Omega_{shed}$: $$\frac{R}{R(\theta)} = \frac{\sin(\theta)}{3\sin(\theta/3)}.$$

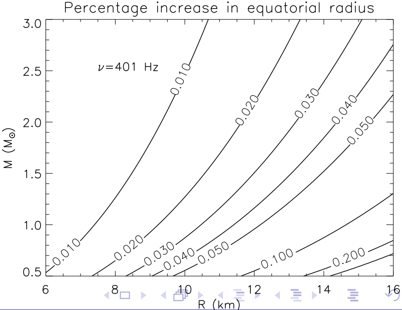

Bulk Matter Energy and Pressure

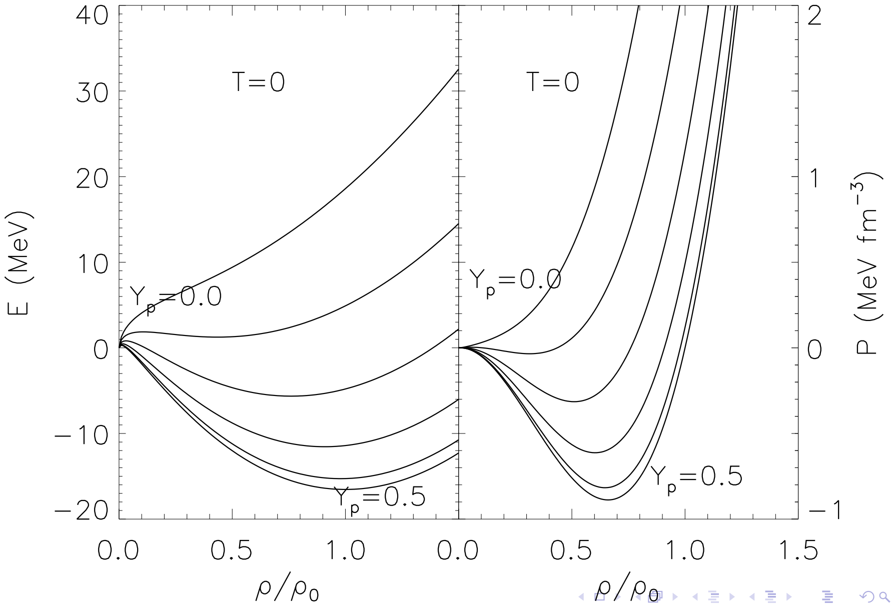

Schematic Free Energy Density

$F(n, x, T)$; n: number density; x: proton fraction; T: temperature

$n_s \simeq 0.16 \pm 0.01$ fm^{-3}: nuclear saturation density
$B \simeq 16 \pm 1$ MeV: saturation binding energy
$K_s \simeq 240 \pm 20$ MeV: incompressibility
$J \simeq 30 \pm 6$ MeV: bulk symmetry energy
$L \simeq 60 \pm 60$ MeV: symmetry stiffness
$a \simeq 0.065 \pm 0.010$ MeV^{-1}: bulk level density parameter

$K_s' \simeq -200 \pm 200$ MeV: skewness

$K_{sym} \simeq -300 \pm 300$ MeV: symmetry incompressibility

$$F = n\left[-B + \frac{K}{18}\left(1 - \frac{n}{n_s}\right)^2 + J\frac{n}{n_s}(1-2x)^2 - a\left(\frac{n_s}{n}\right)^{2/3} T^2\right]$$

$$P = n^2\frac{\partial(F/n)}{\partial n} = \frac{n^2}{n_s}\left[\frac{K}{9}\left(\frac{n}{n_s} - 1\right) + J(1-2x)^2\right] + \frac{2an}{3}\left(\frac{n_s}{n}\right)^{2/3} T^2$$

$$\mu_n = \frac{\partial F}{\partial n} - \frac{x}{n}\frac{\partial F}{\partial x}$$

$$= -B + \frac{K}{18}\left(1 - \frac{n}{n_s}\right)\left(1 - 3\frac{n}{n_s}\right) + 2J\frac{n}{n_s}(1-2x) - \frac{a}{3}\left(\frac{n_s}{n}\right)^{2/3} T^2$$

$$\hat{\mu} = -\frac{1}{n}\frac{\partial F}{\partial x} = \mu_n - \mu_p = 4J\frac{n}{n_s}(1-2x)$$

$$s = -\frac{1}{n}\frac{\partial F}{\partial T} = 2a\left(\frac{n_s}{n}\right)^{2/3} T; \qquad \varepsilon = F + nTs$$

Phase Coexistence

Negative pressure: matter is unstable to separating into two phases of different densities (and possibly proton fractions). Physically, this represents coexistence of nuclei and vapor. Neglecting finite-size effects, bulk coexistence approximates the EOS at subnuclear densities.

Free Energy Minimization With Two Phases

$$\begin{aligned} F &= \epsilon - nTs = uF_I + (1-u)F_{II}, \\ n &= un_I + (1-u)n_{II}, \\ nY_e &= ux_In_I + (1-u)x_{II}n_{II}. \end{aligned}$$

$$n_{II} = \frac{n - un_I}{1-u}, \qquad x_{II} = \frac{nY_e - un_Ix_I}{n - un_I}$$

$$\begin{aligned} \frac{dF}{dn_I} &= u\frac{\partial F_I}{\partial n_I} + (1-u)\frac{\partial F_{II}}{\partial n_{II}}\left(\frac{-u}{1-u}\right) = u(\mu_{n,I} - \mu_{n,II}) \\ \frac{dF}{dx_I} &= u\frac{\partial F_I}{\partial x_I} + (1-u)\frac{\partial F_{II}}{\partial x_{II}}\left(\frac{-un_I}{n-un_I}\right) = un_I(\hat\mu_I - \hat\mu_{II}) \\ \frac{dF}{du} &= F_I - F_{II} + (1-u)\left[\frac{\partial F_{II}}{\partial n_{II}}\left(\frac{n_{II}-n_I}{1-u}\right) + \frac{\partial F_{II}}{\partial x_{II}}\left(\frac{-un_I}{n-un_I}\right)\right] \end{aligned}$$

$$\Longrightarrow \mu_{nI} = \mu_{nII}\,, \qquad \mu_{pI} = \mu_{pII}\,, \qquad P_I = P_{II}$$

Critical Point
$(Y_e = 0.5)$

$$\left(\frac{\partial P}{\partial n}\right)_T = \left(\frac{\partial^2 P}{\partial n^2}\right)_T = 0$$

$$n_c = \frac{5}{12} n_s$$

$$T_c = \left(\frac{5}{12}\right)^{1/3} \left(\frac{5K}{32a}\right)^{1/2}$$

$$s_c = \left(\frac{12}{5}\right)^{1/3} \left(\frac{5Ka}{8}\right)^{1/2}$$

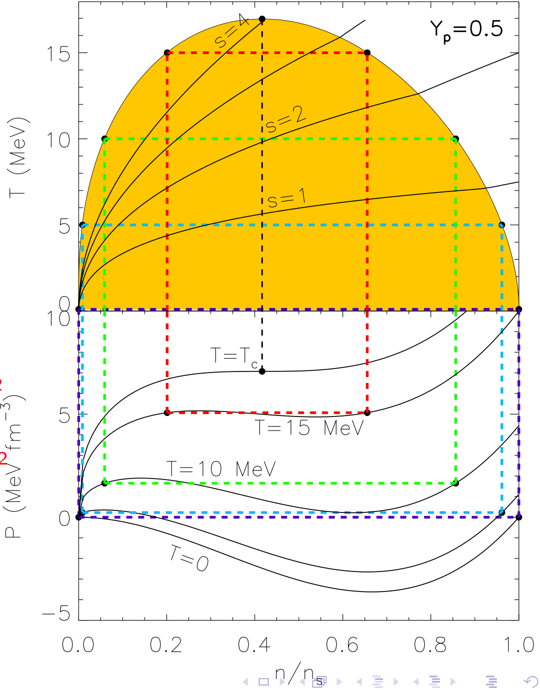

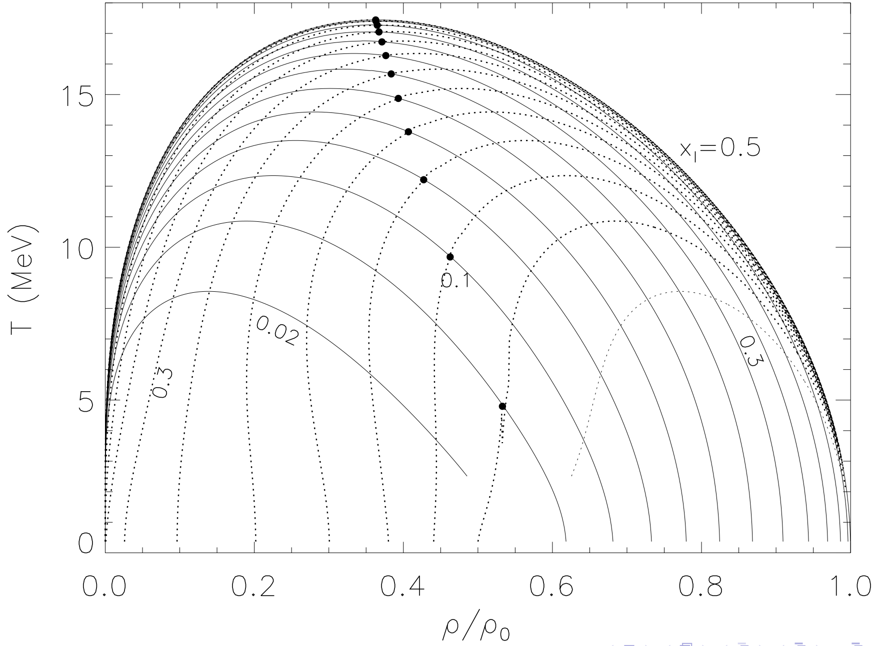
x_l=0.5
0.1
0.02
0.3
0.3
T (MeV)
ρ/ρ0
0.0
0.2
0.4
0.6
0.8
1.0
0
5
10
15

Nuclear Symmetry Energy

Defined as the difference between energies of pure neutron matter ($x = 0$) and symmetric ($x = 1/2$) nuclear matter.

$$S(\rho) = E(\rho, x = 0) - E(\rho, x = 1/2)$$

Expanding around saturation density (ρ_s) and symmetric matter ($x = 1/2$)

$$E(\rho, x) = E(\rho, 1/2) + (1 - 2x)^2 S_2(\rho) + \cdots$$

$$S_2(\rho) = \mathbf{J} + \frac{\mathbf{L}}{3} \frac{\rho - \rho_s}{\rho_s} + \cdots$$

$$\mathbf{J} \simeq 31 \text{ MeV}, \mathbf{L} \simeq 50 \text{ MeV}$$

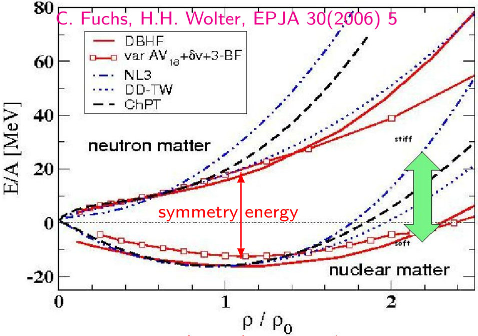

Connections to neutron matter:

$$E(\rho_s, 0) \approx J + E(\rho_s, 1/2) = J - B, \qquad p(\rho_s, 0) = L\rho_s/3$$

Neutron star matter (in beta equilibrium):

$$\frac{\partial(E + E_e)}{\partial x} = 0, \quad p(\rho_s, x_\beta) \simeq \frac{L\rho_s}{3}\left[1 - \left(\frac{4J}{\hbar c}\right)^3 \frac{4 - 3J/L}{3\pi^2 \rho_s}\right]$$

The Liquid Drop Model of Nuclei

$$E(Z,N) \simeq -BA + JAI^2 + (E_s - S_s I^2)A^{2/3} + E_C \frac{Z^2}{A^{1/3}}$$

$B \simeq 16$ MeV, $J \simeq 30$ MeV, $E_s \simeq 18$ MeV, $S_s \simeq 45$ MeV, $E_C \simeq 0.75$ MeV.

At each density, the preferred nucleus has a mass determined by

$$\left(\frac{\partial(E/A)}{\partial A}\right)_x = -\frac{E_s - S_s I^2}{3A^{4/3}} + \frac{2E_C x^2}{3A^{1/3}} = 0$$

. The Nuclear Virial Theorem is

$$E_s - S_s I^2 = 2E_C x^2 A, \qquad A_{opt} = 2\frac{E_s - S_s I^2}{E_C(1-I)^2} \simeq 48(1+2I) \simeq 61.$$

At low densities, the optimum nucleus has a charge determined by

$$\left(\frac{\partial(E/A)}{\partial x}\right)_A = -4I\left(J - \frac{S_s}{A^{1/3}}\right) + (1-I)E_C A^{2/3} = 0,$$

$$I = \frac{E_C A}{4(JA^{1/3} - S_s) + E_C A} \simeq 0.125; \qquad Z \simeq 27$$

Isolated Nuclei

The binding energy curve is heavily skewed. Certain closed-shell nuclei (He, C, O, Pb) have much larger binding than the average.

The optimum value of *I* increases with mass number *A*. This trend represents the *Valley of Beta Stability*.

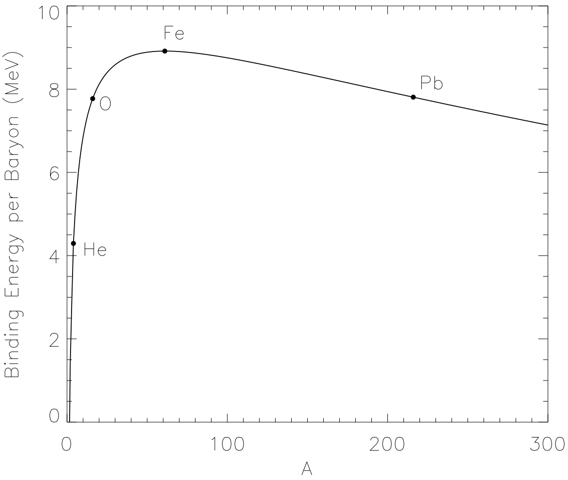

Nuclei at Higher Densities

At the end of stellar evolution, when an iron core forms, the central stellar density is about $\rho \simeq 10^7$ g cm^{-3}, implying a filling factor $u = \rho/\rho_s \simeq 3.7 \cdot 10^{-8}$. The intranuclear spacing is about $2u^{-1/3} \simeq 600$ nuclear radii.

Electron screening reduces the nuclear Coulomb energy.

Approximating electrons as uniformly distributed, even within nuclei, the nuclear Coulomb energy is:

$$E_C = \frac{3}{5}\frac{Z^2 e^2}{R}\left(1 - \frac{3}{2}u^{1/3} + \frac{u}{2}\right)$$

The reduction factor is about 0.5% for $\rho \simeq 10^7$ g cm^{-3}.

This effect increases the nuclear mass, which is proportional to E_C^{-1}, as the average density increases.

The optimum I also increases with density due to *beta equilibrium*:

$$\frac{\partial(E/A + E_e)}{\partial x} = -\mu_n + \mu_p + \mu_e = 0.$$

Chemical Potentials and Neutron Drip

Chemical potentials are equivalent to the separation energies:

$$\mu_n = \left(\frac{\partial(E/A)}{\partial N}\right)_Z, \qquad \mu_p = \left(\frac{\partial(E/A)}{\partial Z}\right)_N,$$

$$\mu_e = \frac{\partial(E_e n Y_e)}{\partial(n Y_e)} = \hbar c(3\pi^2 n_s u x)^{1/3}, \qquad Y_e = x,$$

$$\mu_n - \mu_p = -\left(\frac{\partial(E/A)}{\partial x}\right)_A,$$

At sufficiently high density, about $\rho = (3.5 - 4) \cdot 10^{11}$ g cm^{-3}, as x becomes smaller and A becomes larger, μ_n becomes positive. Neutrons thus 'drip' out of nuclei.

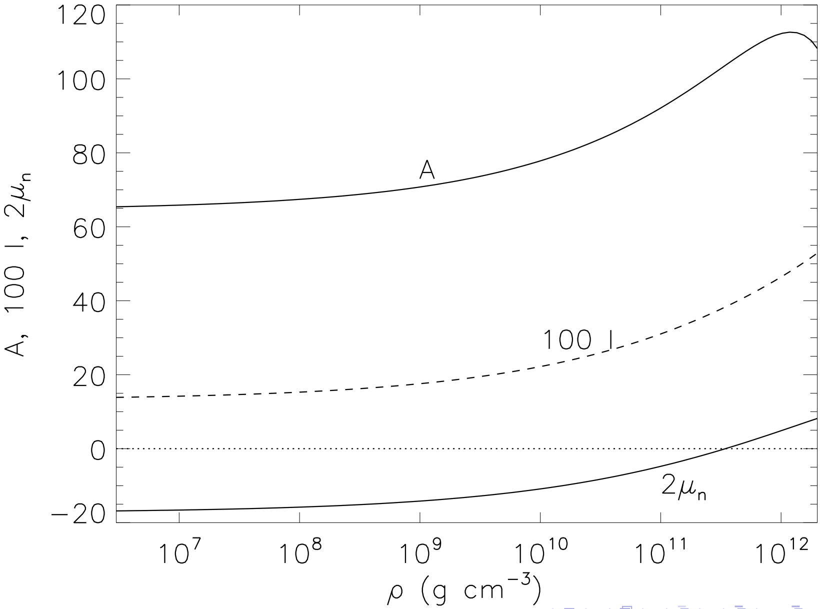
120
100
80
60
40
20
0
−20
A, 100 I, 2μn
A
100 I
2μn
10^7
10^8
10^9
10^10
10^11
10^12
ρ (g cm^−3)

Nuclear Droplet Model

Myers & Swiatecki droplet extension: consider the variation of the neutron/proton asymmetry within the nuclear surface.

$$E(A,Z) = (-B + J\delta^2)(A - N_s) + (E_s - S_s\delta^2)A^{2/3} + E_C Z^2 A^{-1/3} + \mu_n N_s.$$

N_s is the number of excess neutrons associated with the surface, $\delta = 1 - 2x = (A - N_s - 2Z)/(A - N_s)$ is the asymmetry of the nuclear bulk fluid, and $\mu_n = -a_v + J\delta(2-\delta)$ is the neutron chemical potential. Surface tension is the surface thermodynamic potential; adding $\mu_n N_s$ gives the total surface energy. Optimizing $E(A,Z)$ with respect to N_s yields

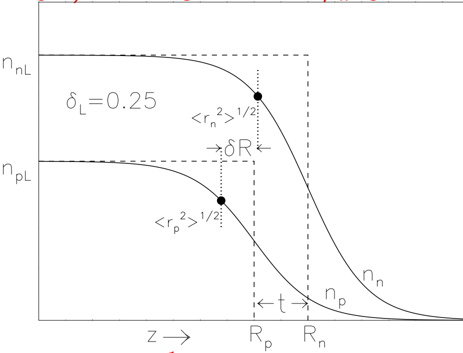

$$N_s = \frac{S_s}{J}\frac{\delta}{1-\delta} = A\frac{I-\delta}{1-\delta}, \quad \delta = I\left(1 + \frac{S_s}{JA^{1/3}}\right)^{-1},$$

$$E(A,Z) = -BA + E_s A^{2/3} + E_C Z^2/A^{1/3} + JAI^2\left(1 + \frac{S_s}{JA^{1/3}}\right)^{-1}.$$

Nuclear Experimental Constraints

Binding Energies

Liquid Droplet Model

$$E_{sym} = AI^2 \left[\frac{J}{1+S_s A^{-1/3}/J} - \frac{Ze^2}{20R} \frac{S_s A^{-1/3}/S_v}{1+S_s A^{-1/3}/J} + \cdots \right]$$

$$\frac{S_s}{J} \simeq \frac{3a}{2r_o} \left[1 + \frac{L}{3J} + \left(\frac{L}{3J} \right)^2 \cdots \right]$$

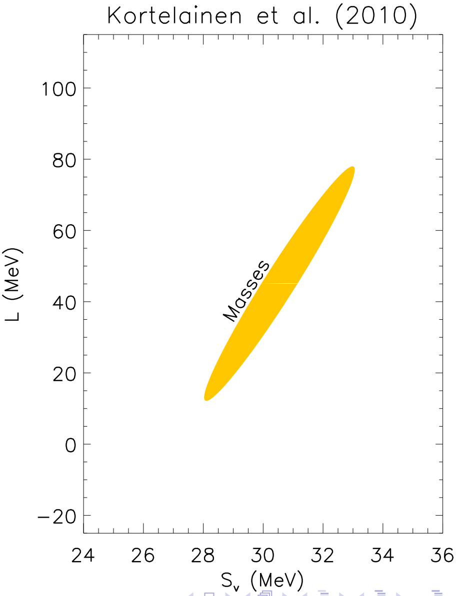

Why Symmetry Parameters are Highly Correlated

Assuming approximate validity of liquid drop model:

$$E_{\rm sym}(N,Z) = (JA - S_s A^{2/3}) I^2$$

$$\chi^2 = \frac{1}{\mathcal{N}\sigma_D^2}\sum_{i=1}^{\mathcal{N}}(E_{ex,i} - E_{sym,i})^2$$

$$\chi_{vv} = \frac{2}{\mathcal{N}\sigma_D^2}\sum_{i=1}^{\mathcal{N}} I_i^4 A_i^2 = 61.6\,\sigma_D^{-2}$$

$$\chi_{vs} = -\frac{2}{\mathcal{N}\sigma_D^2}\sum_{i=1}^{\mathcal{N}} I_i^4 A_i^{5/3} = -10.7\,\sigma_D^{-2}$$

$$\chi_{ss} = \frac{2}{\mathcal{N}\sigma_D^2}\sum_{i=1}^{\mathcal{N}} I_i^4 A_i^{4/3} = 1.87\,\sigma_D^{-2}$$

$$\sigma_J = \sqrt{\frac{2\chi_{ss}}{\chi_{vv}\chi_{ss}-\chi_{sv}^2}} \simeq 2.3\,\sigma_D$$

$$\sigma_{S_s} = \sqrt{\frac{2\chi_{vv}}{\chi_{vv}\chi_{ss}-\chi_{sv}^2}} \simeq 13.2\,\sigma_D$$

$$\alpha = \frac{1}{2}\tan^{-1}\frac{2\chi_{vs}}{\chi_{vv}-\chi_{ss}} \simeq 9^\circ.8$$

$$r_{vs} = -\frac{\chi_{vs}}{\sqrt{\chi_{vv}\chi_{ss}}} \simeq 0.997$$

Liquid droplet model:

$$E_{\rm sym}(N,Z) = \frac{JAI^2}{1+(S_s/J)A^{-1/3}}$$

$$S_s \simeq \frac{3a}{2r_o} S_v \left[1 + (L/3J) + (L/3J)^2 + \cdots\right]$$

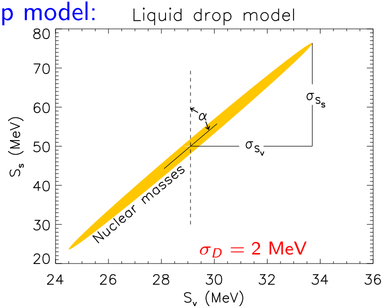

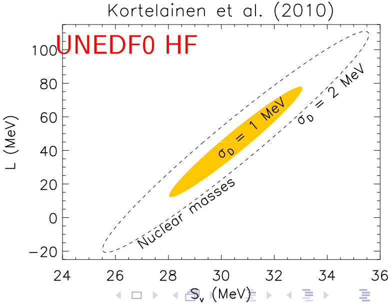

Meaning of $J - L$ Correlation

The slope dL/dJ is an indicator of the most sensitive density u_s for the measurement of the symmetry energy $S(u)$.

If the correlation line goes through (J, L), a change dJ can be compensated by a change dL.

$$\frac{dJ}{dL} = -\left(\frac{\partial S(u_s)}{\partial L}\right)_J \bigg/ \left(\frac{\partial S(u_s)}{\partial J}\right)_L .$$

Example: $S(u) = S_K u^{2/3} + S_V u^\gamma, \quad S_K \simeq 12.5 \text{ MeV}$
$J = S_K + S_V, \quad L = 2S_K + 3\gamma J = S_K(2 - 3\gamma) + 3\gamma J$

$$\frac{dJ}{dL} = -\frac{\ln u_s}{3}, \quad u_s = \exp\left(-3\frac{dJ}{dL}\right).$$

For binding energies, $dL/dJ \simeq 11, \quad u_s \simeq 0.76$.

Saturation Properties of Nuclear Interactions

Empirical Saturation Window

$B = 16.06 \pm 0.20$ MeV

$n_s = 0.1558 \pm 0.0054$ fm^{-3}

$K_{1/2} = 236.5 \pm 15.4$ MeV

Data from Dutra (2012, 2014)

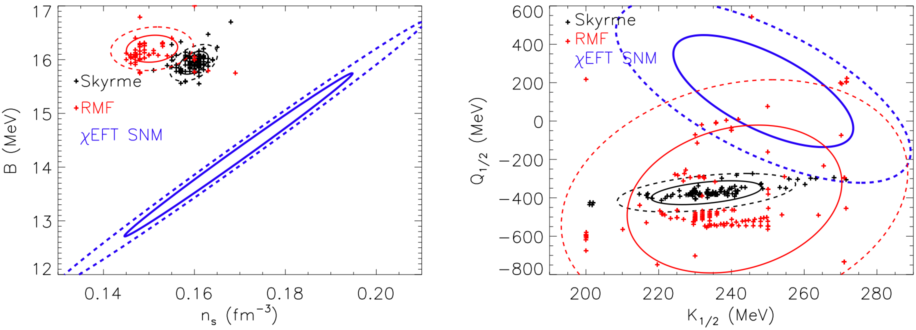

Theoretical Neutron Matter Studies

Recently developed chiral effective field theory allows a systematic expansion of nuclear forces at low energies based on the symmetries of quantum chromodynamics. It exploits the gap between the pion mass (the pseudo-Goldstone boson of chiral symmetry-breaking) and the energy scale of short-range nuclear interactions established from experimental phase shifts. It provides the only known consistent framework for estimating energy uncertainties.

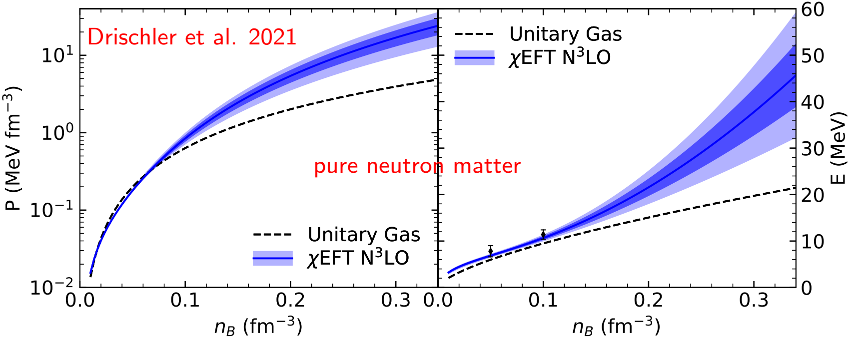

Symmetry Parameters From Chiral EFT

Two approaches to ext

1. Take the difference between pure neutron and symmetric matter energies and pressures at the calculated saturation density.

2. Use pure neutron matter energy and pressure with the empirical saturation window from nuclear mass fits. $J = E_N(n_s) + B$, $L = 3P_N(n_s)/n_s$.

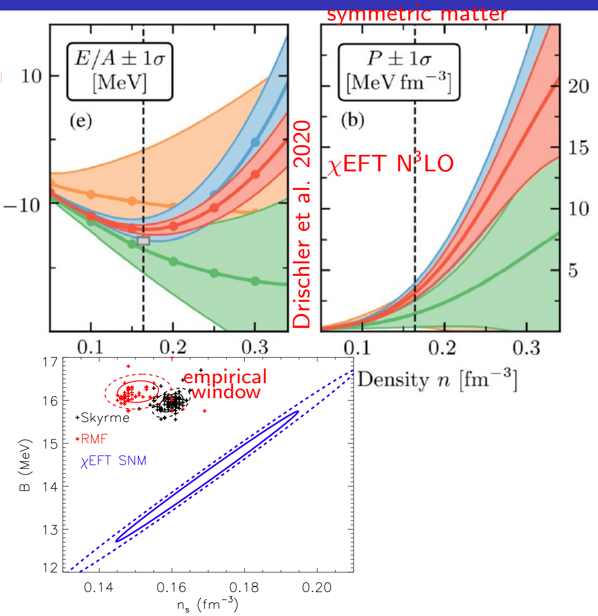

Symmetry Parameters From Neutron Matter

Pure neutron matter calculations are more reliable than symmetric matter calculations.

Symmetric matter emerges from a delicate cancellation sensitive to short- and intermediate-range three-body interactions at N^2LO that are Pauli-blocked in pure neutron matter.

N^3LO symmetric matter calculations don't saturate within empirical ranges for n_s and B,

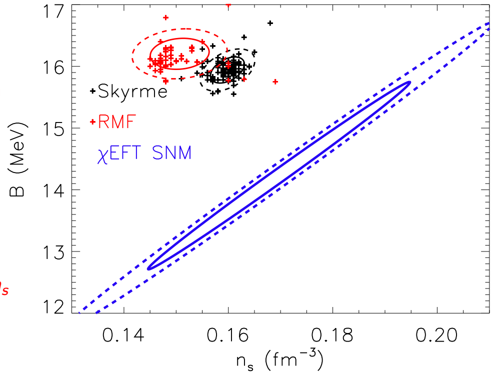

and introduce spurious correlations in symmetric matter.

We infer symmetry parameters from $E_N(n_s)$ and $P_N(n_s)$ using

$$J = E_N(n_s) + B$$

$$L = 3P_N(n_s)/n_s$$

and include uncertainties in E_N, P_N, n_s and B.

Correlations From Chiral EFT

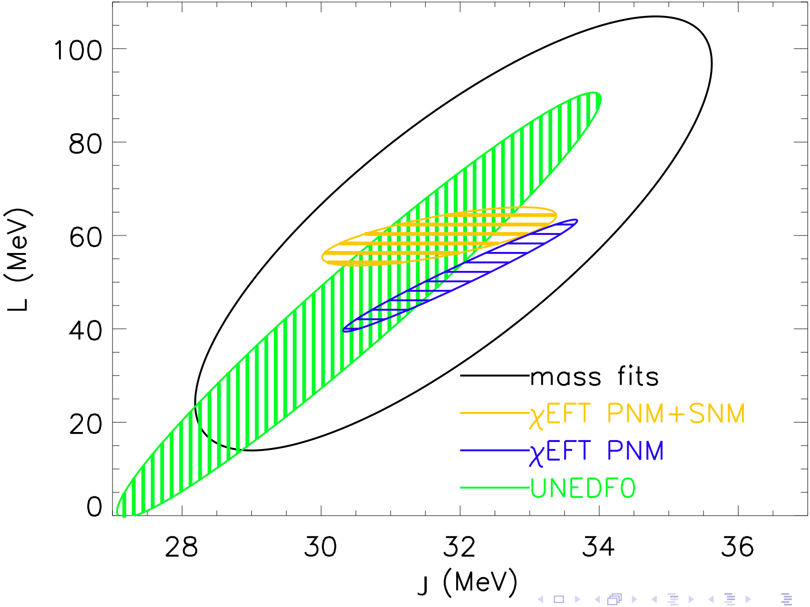

Bounds From The Unitary Gas Conjecture

The Conjecture (UGC):
Neutron matter energy always larger than unitary gas energy.
$E_{UG} = \xi_0(3/5)E_F$, or

$$E_{UG} \simeq 12.6 \left(\frac{n}{n_s}\right)^{2/3} \text{MeV}.$$

The unitary gas consists of fermions interacting via a pairwise short-range s-wave interaction with infinite scattering length and zero range. Cold atom experiments show a universal behavior with the Bertsch parameter $\xi_0 \simeq 0.37$.

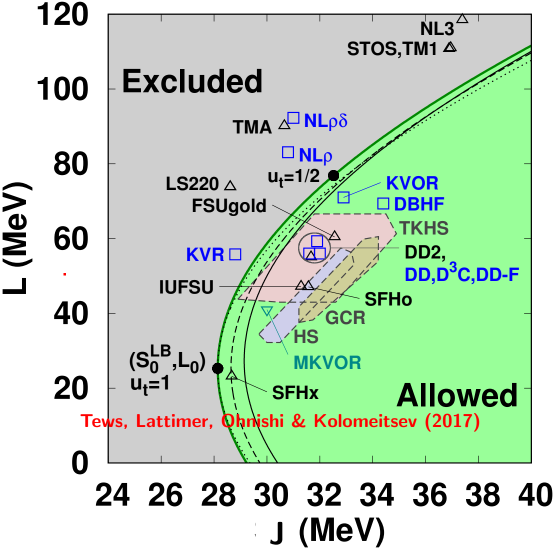

For $n \geq n_s$, one also observes $P_N > P_{UG}$ (UGPC).
$J \geq 28.6$ MeV; $L \geq 25.3$ MeV; $P_N(n_s) \geq 1.35$ MeV fm^{-3}; $R_{1.4} \geq 9.7$ km

Applying Unitary Gas Constraints

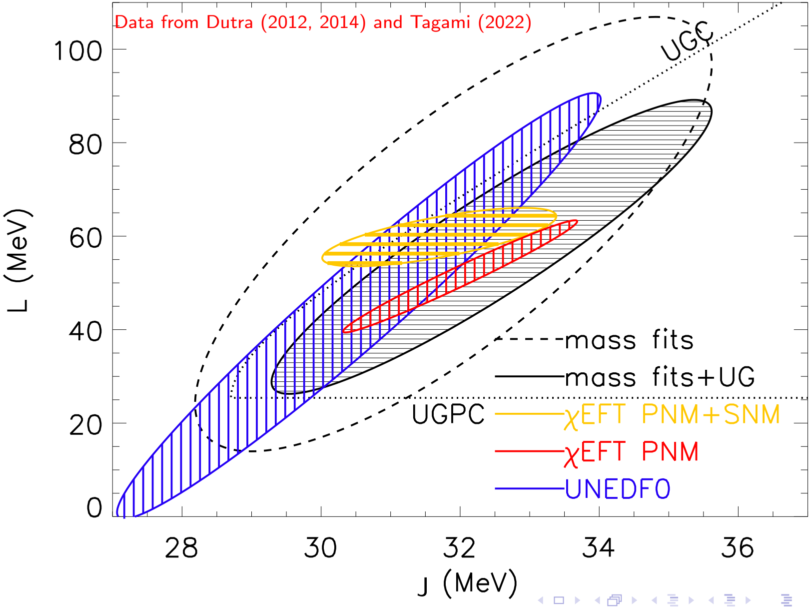

Neutron Skin Thickness

The difference between the mean neutron and proton radii in the liquid droplet model is

$t_{np} = R_n - R_p$.

The mean square difference is

$r_{np}^2 =< R_n >^2 - < R_p >^2$.

$$r_{np} = \sqrt{\frac{3}{5}\frac{2r_o I}{3}\frac{S_s}{J}}\left[1 + S_s A^{-1/3}/J\right]^{-1} f_C$$

Implies strong $L - r_{np}$ correlation.

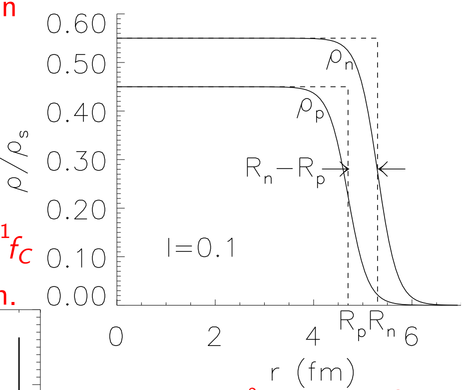

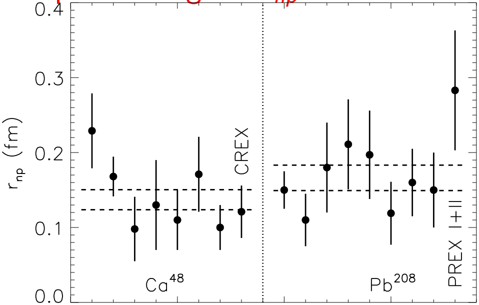

$$f_C = 1 - \frac{3Ze^2}{140 I S_S r_o}\left(1 + \frac{10 S_S}{3JA^{1/3}}\right)$$

For ^{208}Pb: $r_{np} \simeq 0.13$ fm

$$\frac{\Delta(S_S/J)}{\Delta J} \simeq -0.020$$

$$\frac{\Delta L}{\Delta J} = \frac{\Delta(S_S/J)}{\Delta J}\frac{1}{0.0234} \simeq -0.84$$

Nuclear Experimental Constraints

Neutron Skin Thicknesses

$$r_{np} = \frac{2r_o}{3J}\frac{1}{\sqrt{1-I^2}}(1+S_sA^{-1/3}/J)^{-1}$$
$$\times\sqrt{\frac{3}{5}}\left[IS_s - \frac{3Ze^2}{140r_o}\left(1+\frac{10}{3}\frac{S_sA^{-1/3}}{J}\right)\right]$$

$$r_{np,208} = 0.15 \pm 0.04 \text{ fm}$$

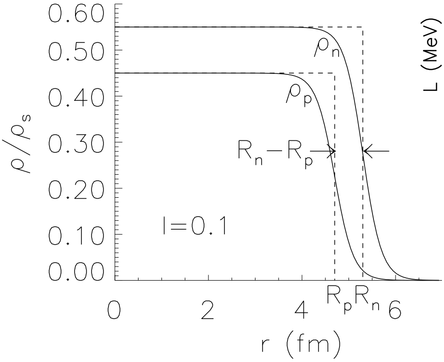

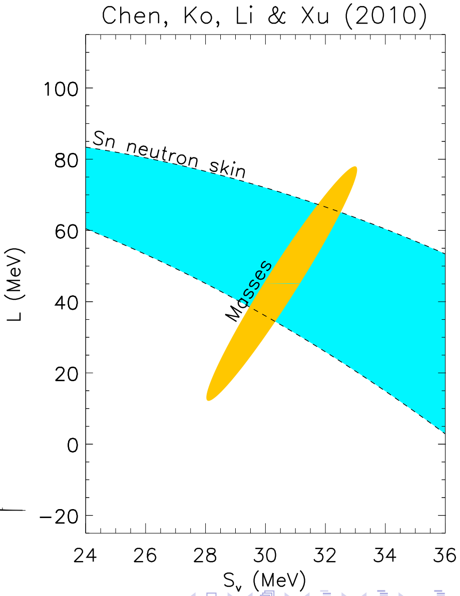

Calculated $L - r_{np}$ Correlations

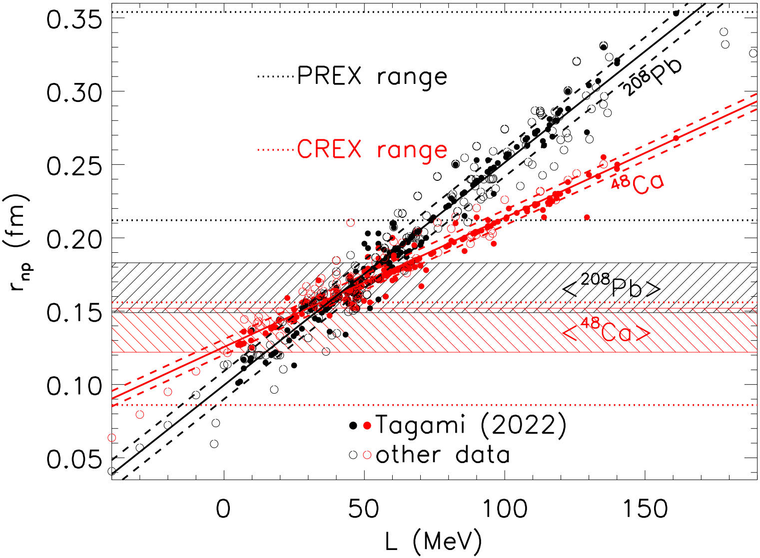

Implied L Values

Historical experimental weighted average ^{208}Pb
$r_{np}^{208} = 0.166 \pm 0.017$ fm, implying $L = 45 \pm 13$ MeV.

Historical experimental weighted average ^{48}Ca
$r_{np}^{48} = 0.137 \pm 0.015$ fm, implying $L = 14 \pm 21$ MeV.

Combined $L = 36 \pm 11$ MeV.

Parity-violating electron scattering measurements at JLab:

PREX I+II ^{208}Pb (Adhikari et al. 2021):
$r_{np}^{208} = 0.283 \pm 0.071$ fm, implying $L = 119 \pm 46$ MeV.

CREX ^{48}Ca (Adhikari et al. 2022):
$r_{np}^{48} = 0.121 \pm 0.035$ fm, implying $L = -5 \pm 42$ MeV.

Combined $L = 51 \pm 31$ MeV.

$r_{np}^{208} - r_{np}^{48}$ Linear Correlation

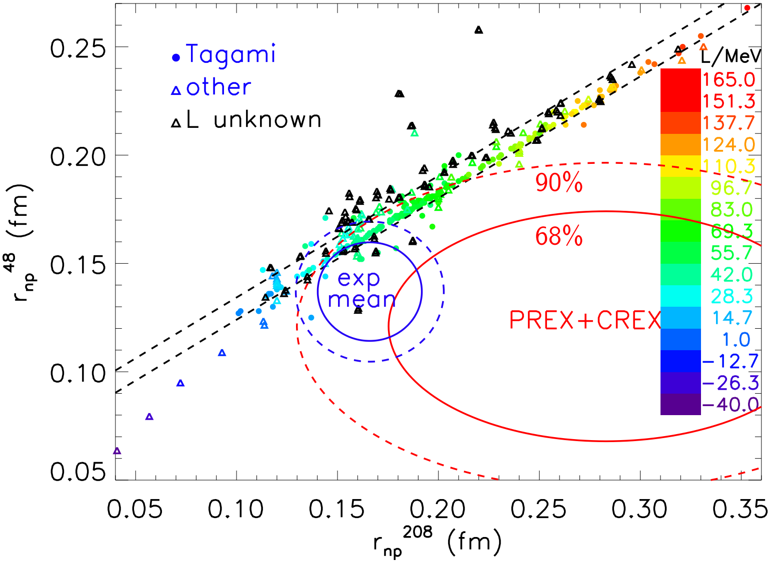

Detail

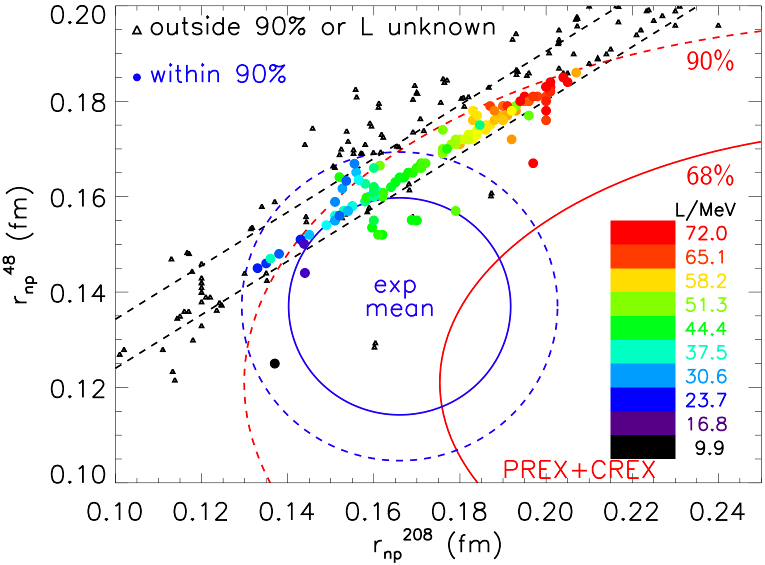

outside 90% or L unknown
within 90%
90%
68%
exp mean
PREX+CREX
L/MeV
72.0
65.1
58.2
51.3
44.4
37.5
30.6
23.7
16.8
9.9
0.20
0.18
0.16
0.14
0.12
0.10
r_{np}^{48} (fm)
0.10 0.12 0.14 0.16 0.18 0.20 0.22 0.24
r_{np}^{208} (fm)

Implied $J - L$

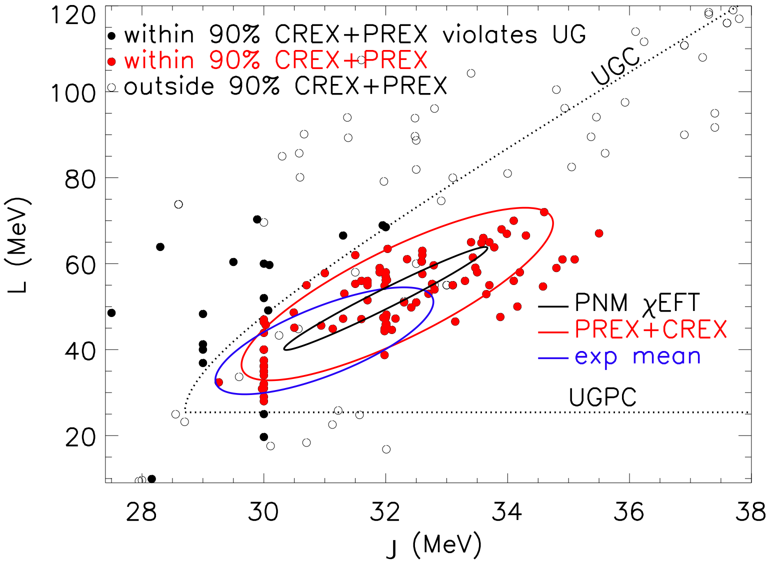

120
100
80
60
40
20
28
30
32
34
36
38
L (MeV)
J (MeV)
within 90% CREX+PREX violates UG
within 90% CREX+PREX
outside 90% CREX+PREX
UGC
UGPC
PNM χEFT
PREX+CREX
exp mean

Implied $R_{1.4} - L$

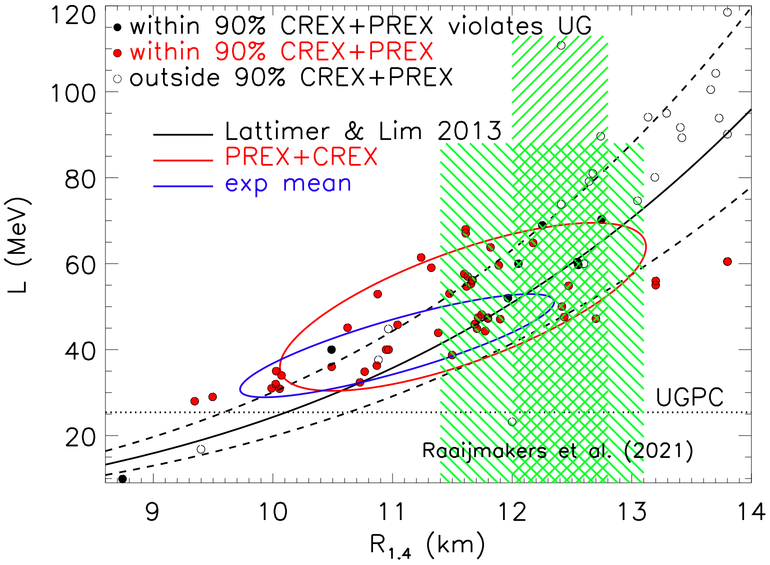

Nuclear Experimental Constraints

Flows in
Heavy Ion Collisions

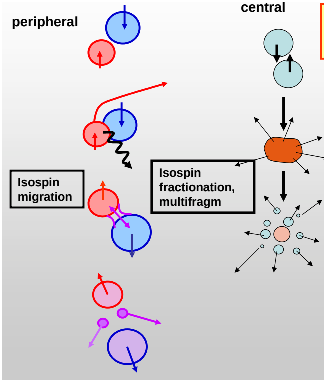

Wolter, NuSYM11

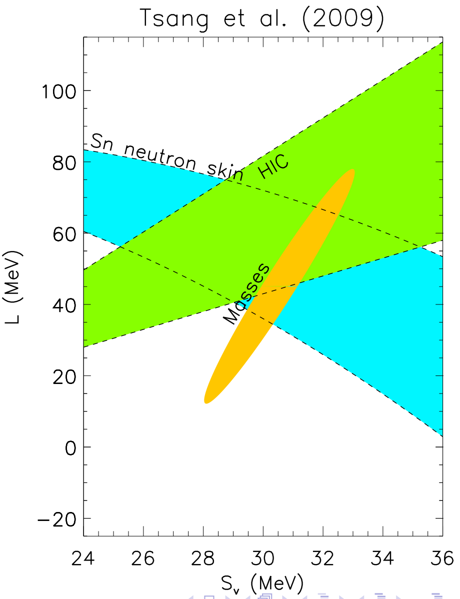

Giant Dipole Resonances

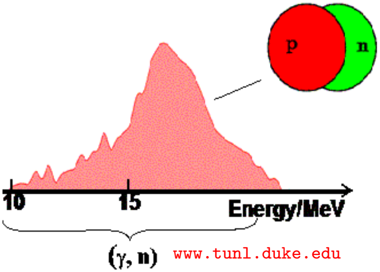

$$E_{-1} \propto \sqrt{\frac{J}{1+\frac{5S_s}{3J}A^{-1/3}}}$$

23.3 MeV$< S_2(0.1\ \mathrm{fm}^{-3}) <$24.9 MeV

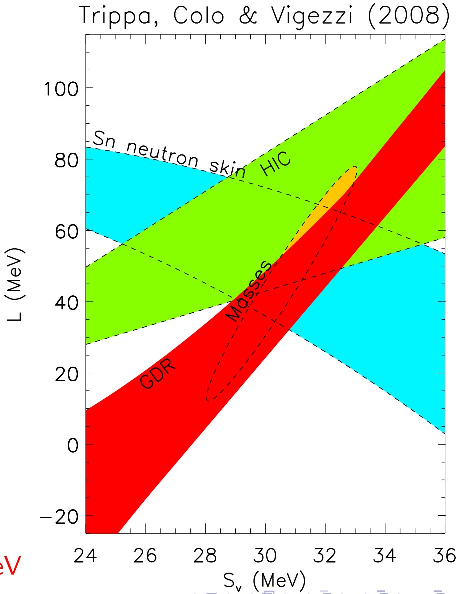

Nuclear Experimental Constraints

Dipole Polarizabilities

$\alpha_D = 4m_{-1}$

$\simeq \frac{AR^2}{20J}\left(1 + \frac{5}{3}\frac{S_s A^{-1/3}}{J}\right)$

Uses data of
Tamii et al. (2011)

$\alpha_{D,208} = 20.1 \pm 0.6\ \mathrm{fm}^2$

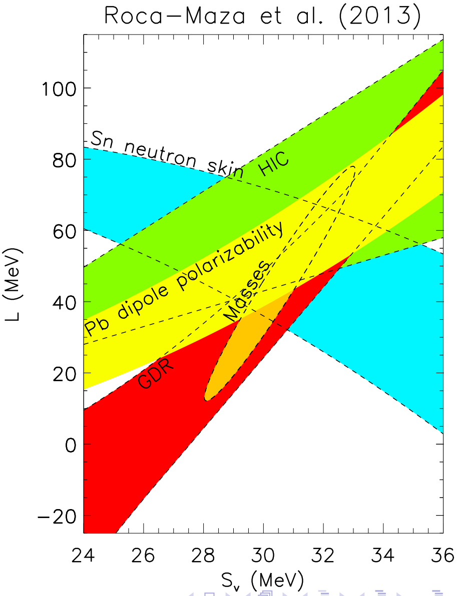

Combined Constraints

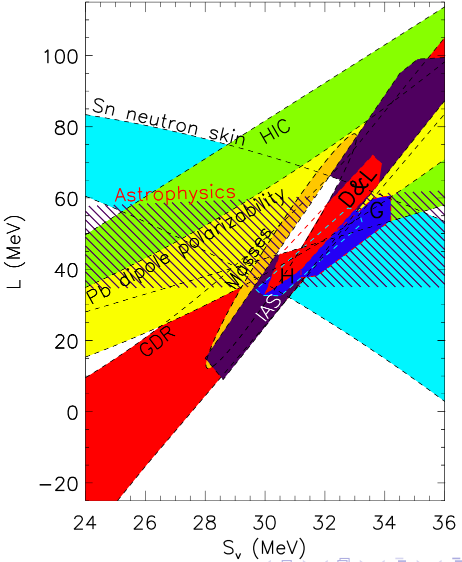

The Discovery of Pulsars

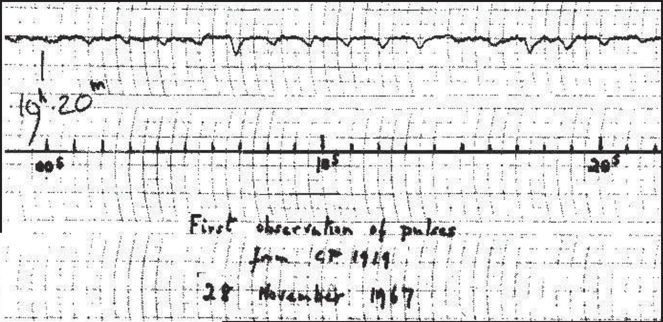

PhD student **Jocelyn Bell** and
Prof. **Antony Hewish**
Initially "**Little Green Men**"
Hewish won Nobel Prize in 1974

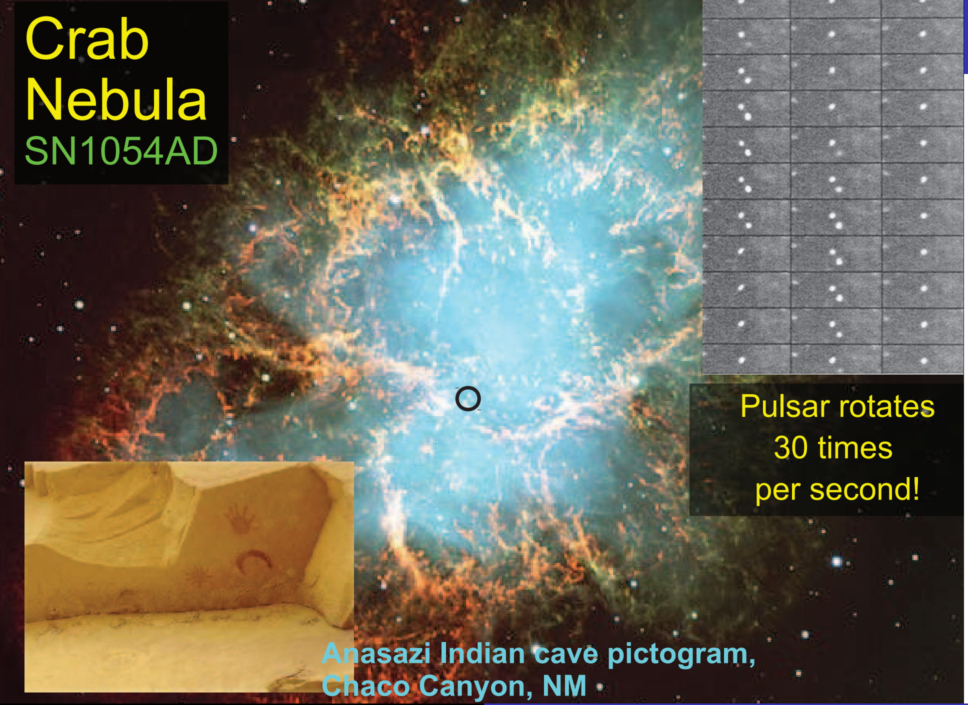
Crab
Nebula
SN1054AD
Pulsar rotates
30 times
per second!
Anasazi Indian cave pictogram,
Chaco Canyon, NM

$P - \dot{P}$ Diagram

$$\tau_c = \frac{P}{2\dot{P}}$$

$$B \simeq 3 \cdot 10^{19}\sqrt{P\dot{P}}\ \mathrm{G}$$

$$-\dot{E} \simeq 10^{47}\frac{\dot{P}}{P^3}\ \mathrm{erg/s}$$

P in seconds

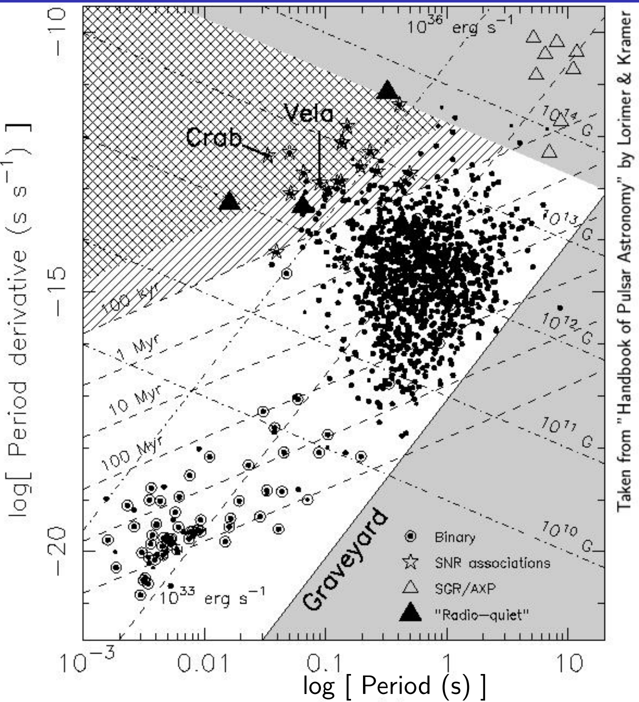

Pulsar Flavors

Young PSRs

(high B, fast spin, very energetic)

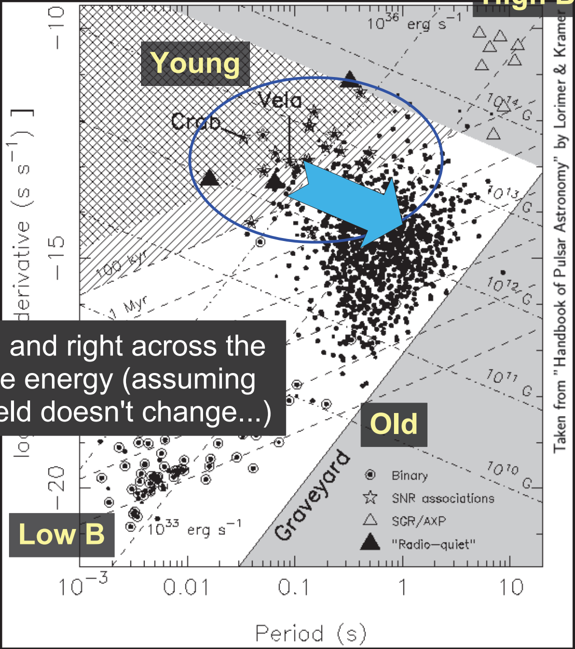

Pulsars move down and right across the diagram as they lose energy (assuming that the magnetic field doesn't change...)

Pulsar Flavors

Young PSRs

(high B, fast spin, very energetic)

Normal PSRs

(average B, slow spin)

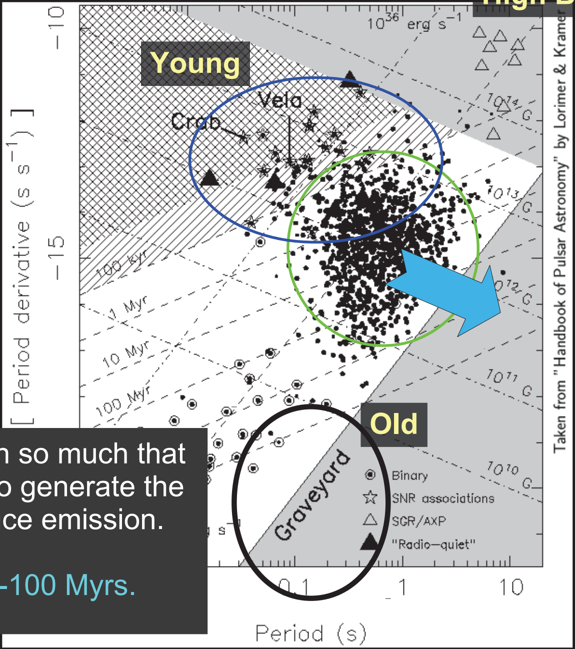

Eventually they slow down so much that there is not enough spin to generate the electric fields which produce emission.

Their lifetimes are 10-100 Myrs.

Millisecond Pulsars: via “Recycling”

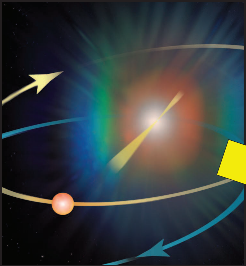

Supernova produces a neutron star

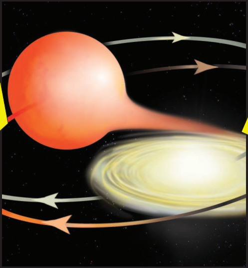

Red Giant transfers matter to neutron star

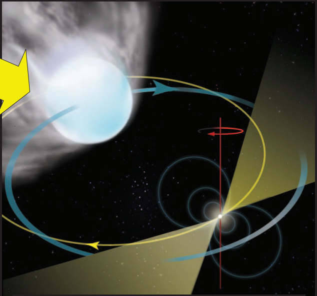

Millisecond Pulsar emerges with a white dwarf companion

Alpar et al 1982
Radhakrishnan & Srinivasan 1984

Picture credits: Bill Saxton, NRAO/AUI/NSF

Pulsar Flavors

Young PSRs
(high B, fast spin, very energetic)

Normal PSRs
(average B, slow spin)

Millisecond PSRs
(low B, very fast, very old, very stable spin, best for basic physics tests)

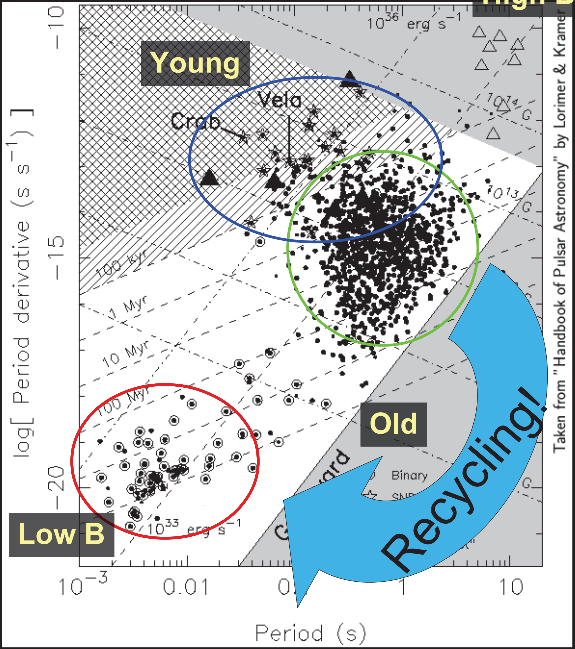

What's a Magnetar?

Neutron stars with extremely strong magnetic fields:

10^{14-15} Gauss

(~1000x stronger than normal PSRs)

Powered by decay of magnetic field, not rotation!

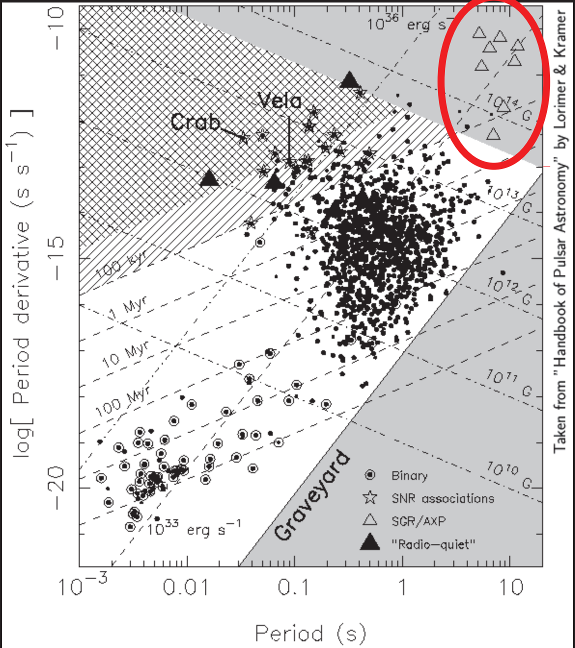

Giant X-ray Flares: Magnetar SGR 1900+14

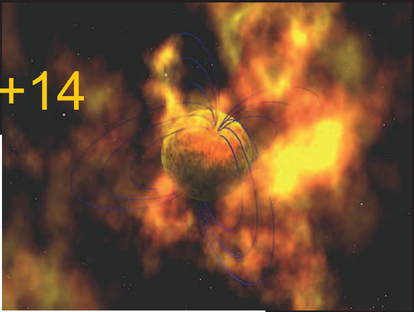

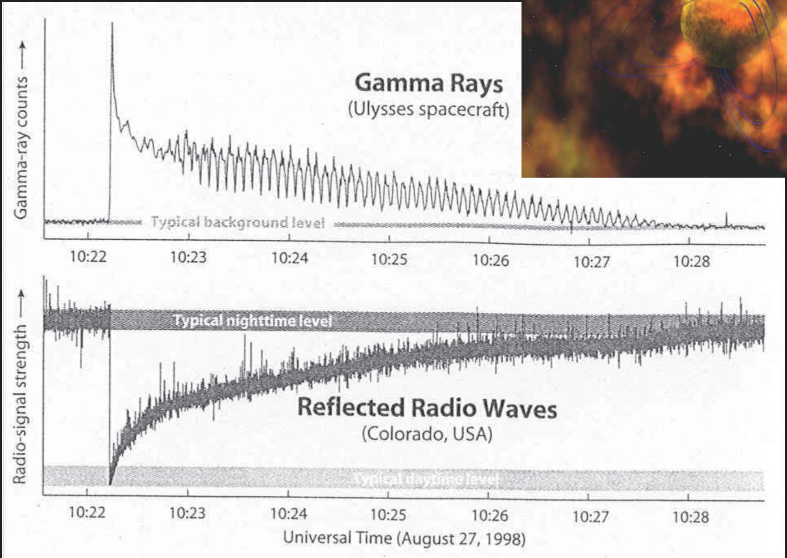

Pulsars are Precise Clocks

PSR J0437-4715

At 00:00 UT Jan 18 2011:

P = 5.7574519420243 ms
+/- 0.0000000000001ms

The last digit changes by 1 every half hour!

This digit changes by 1 every 500 years!

This extreme precision is what allows us to ***use pulsars as tools*** to do unique physics!

Pulsar Timing: *Pulse Phase Tracking*

Unambiguously account for every rotation of a pulsar over years

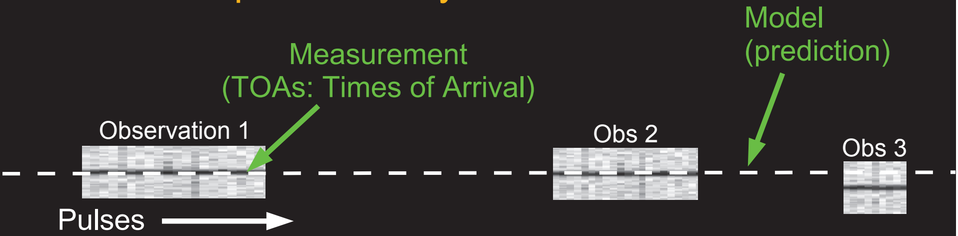

Measurement - Model = Timing Residuals

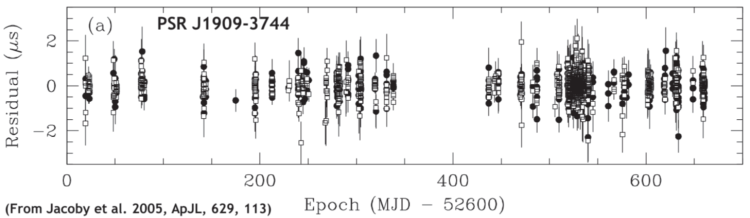

(From Jacoby et al. 2005, ApJL, 629, 113)

200ns RMS over 2 yrs

PSR J0737-3039

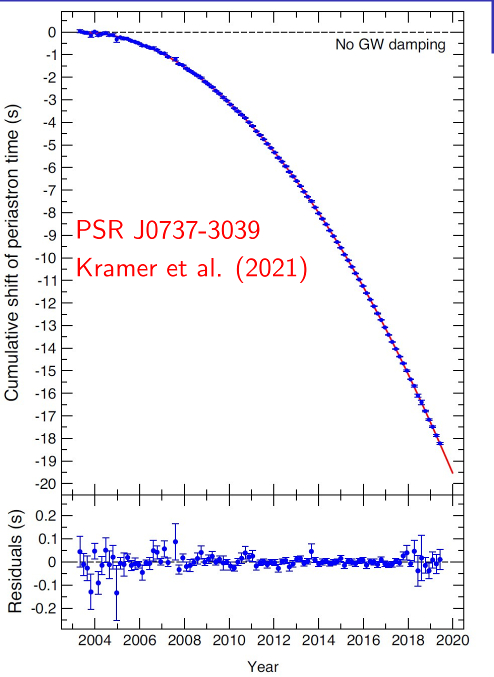

PSR J0737-3039

Kramer et al. (2021)

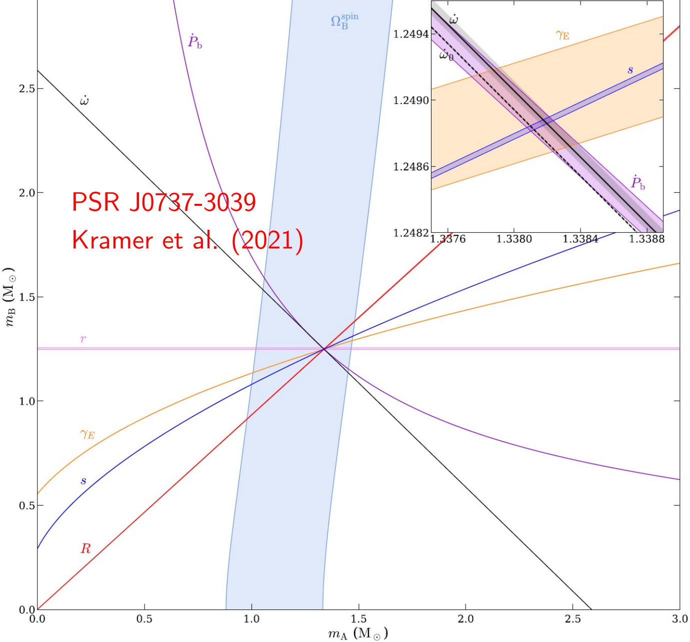

PSR J1614-2230

3.15 ms pulsar in 8.69d orbit with 0.5 $M_\odot$ white dwarf companion.
Shapiro delay tightly confines the edge-on inclination: $\sin i = 0.99984$
Pulsar mass is 1.97 ± 0.04 $M_\odot$
Distance > 1 kpc, $B \simeq 1.8 \times 10^8$ G

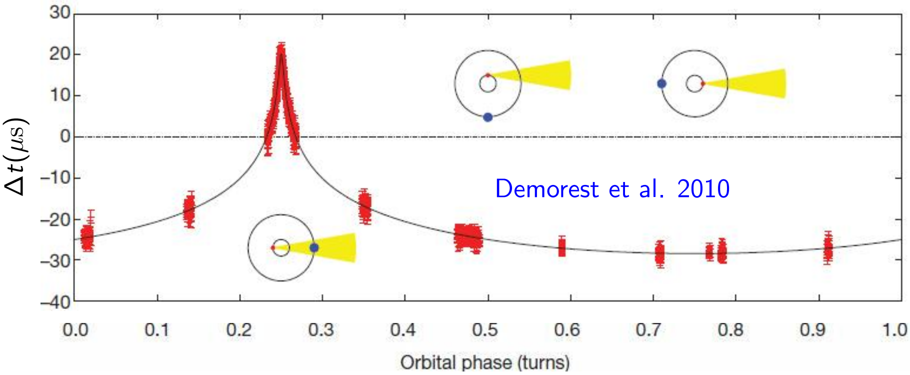

Black Widow Pulsar PSR B1957+20

A 1.6ms pulsar in circular 9.17h orbit with $\sim 0.03\ M_\odot$ companion.
The pulsar is eclipsed for 50-60 minutes each orbit; the eclipsing object has a volume much larger than the secondary or its Roche lobe.
The pulsar is ablating the companion leading to mass loss and the eclipsing plasma cloud. The secondary may nearly fill its Roche lobe.
Ablation by the pulsar leads to secondary's eventual disappearance.
The optical light curve tracks the motion of the secondary's irradiated hot spot rather than its center of mass motion.

pulsar radial velocity

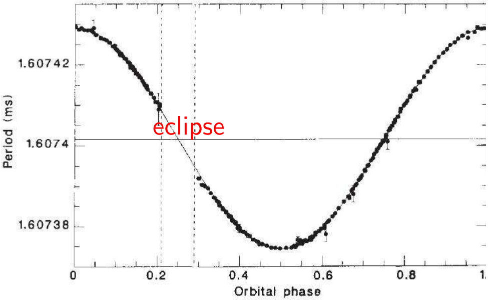

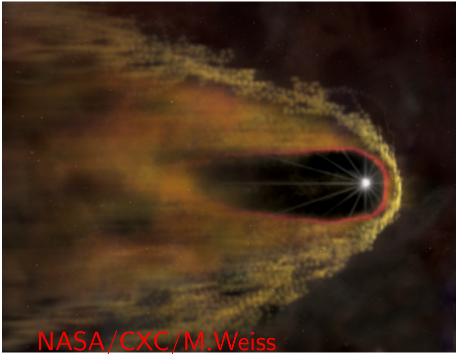

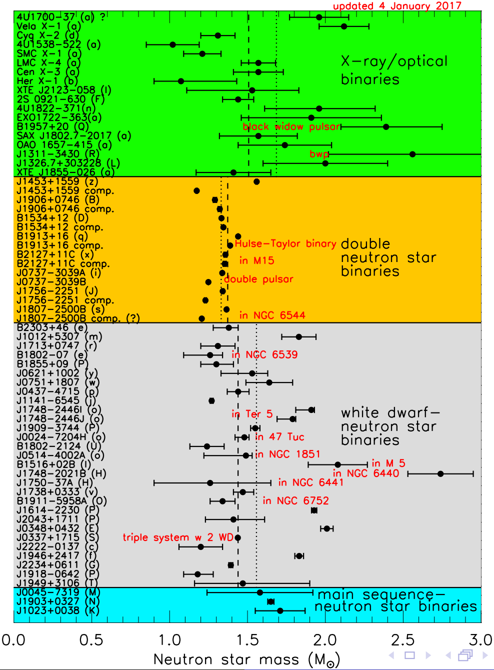

vanKerkwijk 2010

Romani et al. 2012

Although simple average mass of w.d. companions is 0.23 $M_\odot$ larger, weighted average is 0.04 $M_\odot$ smaller

Demorest et al. 2010

Antoniadis et al. 2013

Champion et al. 2008

The Distribution of Neutron Star Masses

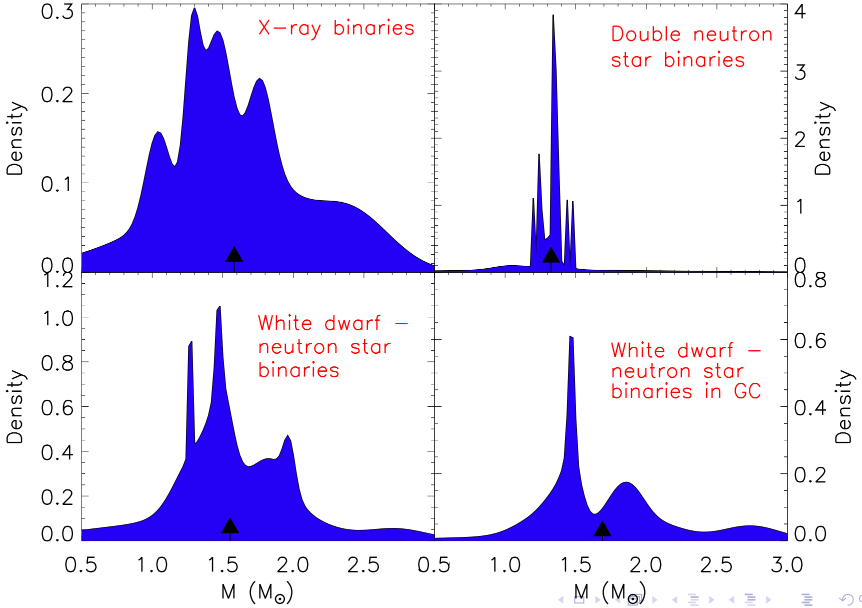

Radiation Radius

- The measurement of flux and temperature yields an apparent angular size (pseudo-BB):

$$\frac{R_\infty}{d} = \frac{R}{d}\frac{1}{\sqrt{1-2GM/Rc^2}}$$

- Observational uncertainties include distance, interstellar H absorption (hard UV and X-rays), atmospheric composition
- Nearby isolated neutron stars (parallax measurable)
- Quiescent X-ray binaries in globular clusters (reliable distances, low B H-atmosperes)
- Bursting sources in which Eddington flux is measured

$$F_{Edd} = \frac{GMc}{\kappa D^2}\sqrt{1-\frac{2GM}{R_{ph}c^2}}$$

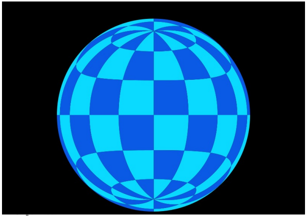

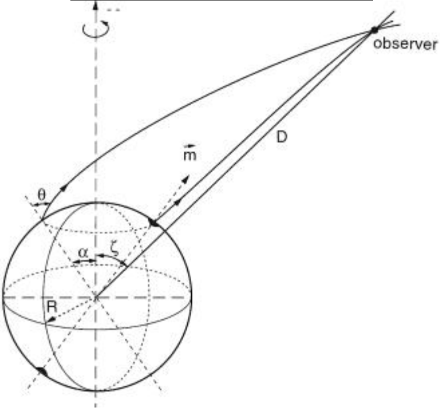

Quiescent Sources in Globulars

Hot neutron stars in globular clusters

- Globular clusters evolve: more massive stars, including binaries, sink to center via long-range stellar encounters.
- Close binaries formed in encounters.
- Episodes of accretion in close binaries heats neutron stars: they are reborn.
- Following accretion, they become quiescent, low-mass X-ray sources.
- Accretion suppresses surface B fields.
- Atmospheric composition is H.

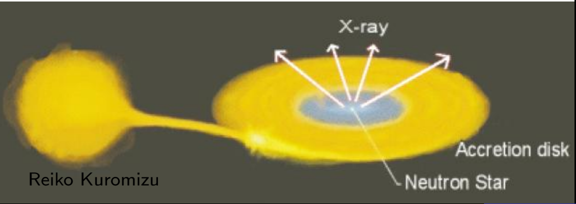

Reiko Kuromizu

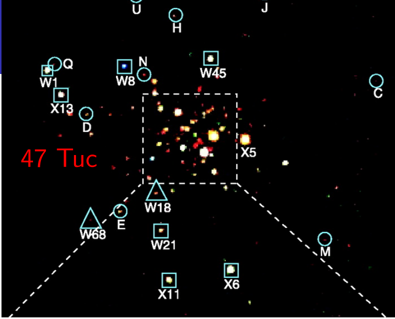

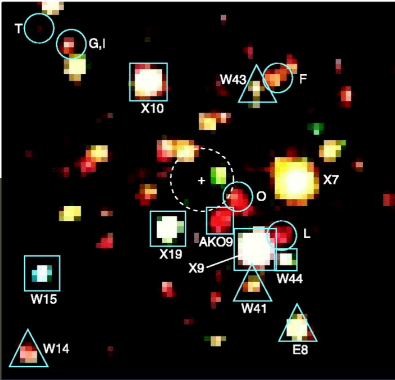

Semi-Universal Relations for Neuton Stars

- The first universal relations discovered for neutron stars connected
  - pressure and neutron star radius,
  - binding energy and compactness,
  - moment of inertia and compactness.
- Simple explanations exist using analytical TOV solutions that bracket realistic equations of state.
- Tolman VII: $\varepsilon = \varepsilon_0 \left[1 - (r/R)^2\right]$;
- Buchdahl: $\varepsilon = 12\sqrt{\varepsilon_* p} - 5p$.
- Easily extended to tidal Love number and rotational quadrupole moment.

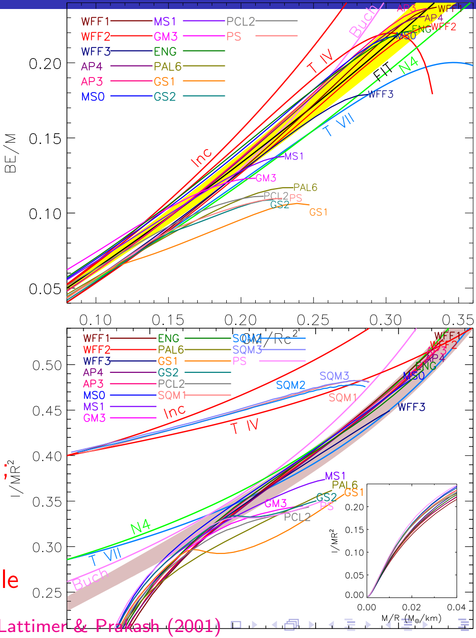

Lattimer & Prakash (2001)

I-Love-Q Correlations

Yagi and Yunes (2013) discovered that the moment of inertia I, the tidal love number (tidal response) λ, and the quadrupole polarizability Q are extremely highly correlated.

Dimensionless love numbers of neutron stars in a merging binary are, furthermore, universally related, allowing for their individual measurements from gravitational waves of a binary inspiral (Yagi and Yunes 2015).

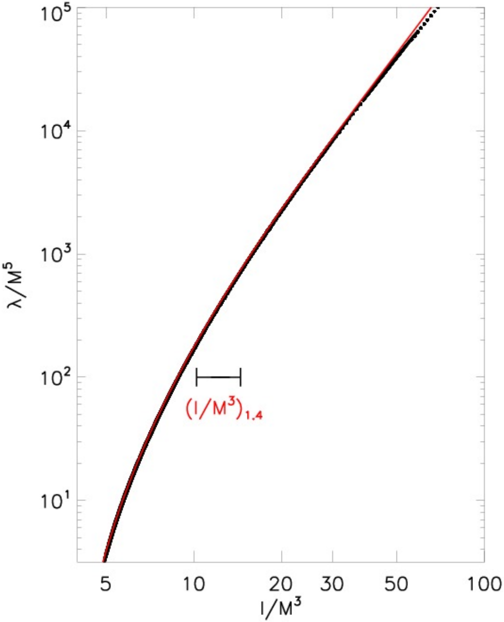

Additional Proposed Radius and Mass Constraints

- Pulse profiles
  Hot or cold regions on rotating neutron stars alter pulse shapes: NICER and LOFT will enable timing and spectroscopy of thermal and non-thermal emissions. Light curve modeling → M/R; phase-resolved spectroscopy → R.
- Supernova neutrinos
  Millions of neutrinos detected from a Galactic supernova will measure BE$= m_B N - M$, $< E_\nu >$, τ_ν.
- QPOs from accreting sources
  ISCO and crustal oscillations
- Gravitational radiation
  Mergers of neutron stars with neutron stars or black holes
  'Mountains' on spinning stars
  R-mode instabilities

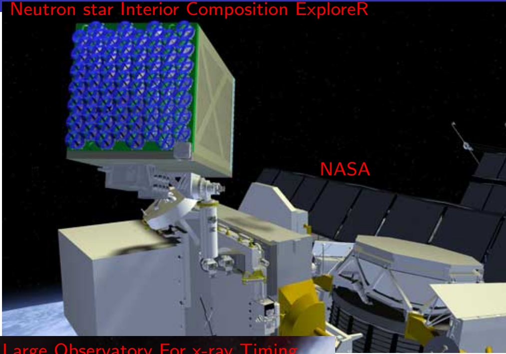

Science Measurements

NICER

Reveal stellar structure through lightcurve modeling, long-term timing, and pulsation searches

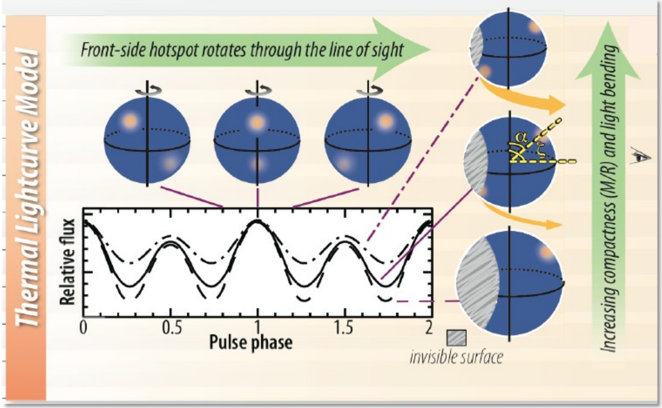

Lightcurve modeling constrains the compactness (M/R) and viewing geometry of a non-accreting millisecond pulsar through the depth of modulation and harmonic content of emission from rotating hot-spots, thanks to gravitational light-bending…

Science Measurements (cont.)

NICER

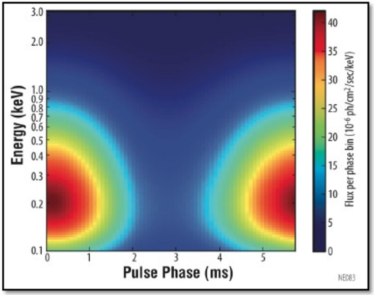

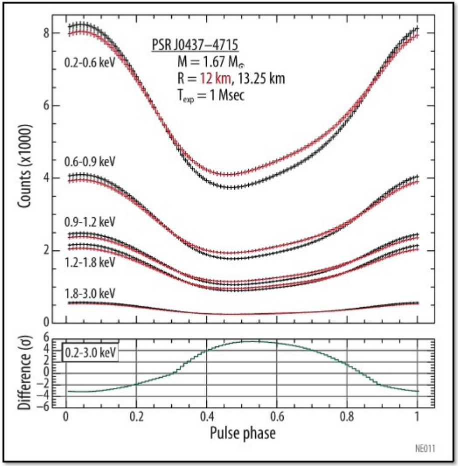

... while phase-resolved spectroscopy promises a direct constraint of radius *R*.

GW170817

- LVC detected a signal consistent with a BNS merger, followed 1.7 s later by a weak gamma-ray burst.
- $\simeq$ 10100 orbits observed over 317 s.
- $\mathcal{M} = 1.186 \pm 0.001\ M_\odot$
- $M_{\rm T,min} = 2^{6/5}\mathcal{M} = 2.725 M_\odot$
- $E_{\rm GW} > 0.025 M_\odot c^2$
- $D_L = 40^{+8}_{-14}$ Mpc
- $75 < \tilde\Lambda < 560$ (90%)
- $M_{\rm ejecta} \sim 0.06 \pm 0.02\ M_\odot$
- Blue ejected mass: $\sim 0.01 M_\odot$
- Red ejected mass: $\sim 0.05 M_\odot$
- Probable r-process production
- Ejecta + GRB: $M_{max} \lesssim 2.22 M_\odot$

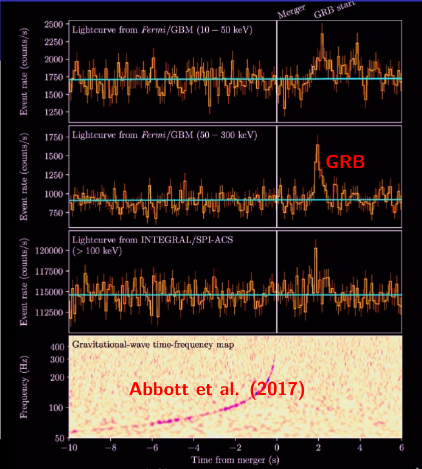

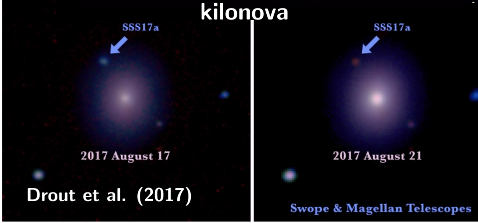

The Effect of Tides

Tides accelerate the inspiral and produce a gravitational wave phase shift compared to the case of two point masses.

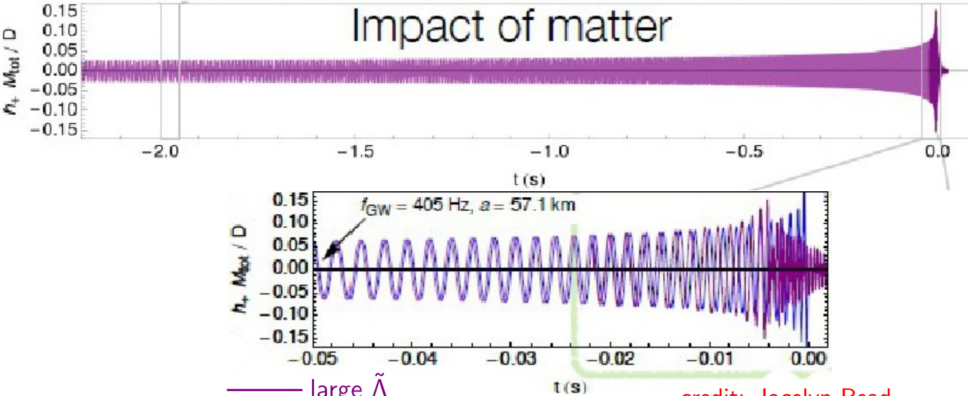

large $\tilde{\Lambda}$

small $\tilde{\Lambda}$

credit: Jocelyn Read

$$\delta\Phi_t = -\frac{117}{256}\frac{(1+q)^4}{q^2}\left(\frac{\pi f_{GW} G\mathcal{M}}{c^3}\right)^{5/3}\tilde{\Lambda} + \cdots .$$

Tidal Deformability

The tidal deformability λ is the ratio of the induced dipole moment Q_{ij} to the external tidal field E_{ij}, $Q_{ij} = -\lambda E_{ij}$.

Use $\beta = GM/Rc^2$ and

$$\Lambda = \frac{\lambda c^{10}}{G^4 M^5} \equiv \frac{2}{3} k_2 \beta^{-5}.$$

$k_2 \propto 1/\beta$ is the dimensionless Love number, so $\Lambda \simeq a\beta^{-6}$. For $1 < M/M_\odot < 1.6$, $a = 0.0093 \pm 0.0007$.

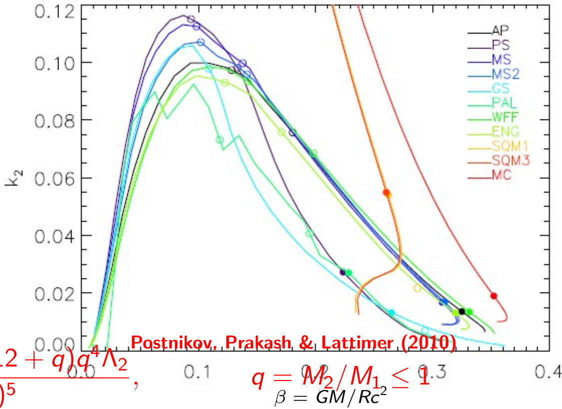

Postnikov, Prakash & Lattimer (2010)

For a neutron star binary, the mass-weighted $\tilde{\Lambda}$ is the relevant observable:

$$\tilde{\Lambda} = \frac{16}{13} \frac{(1+12q)\Lambda_1 + (12+q)q^4\Lambda_2}{(1+q)^5}, \qquad q = M_2/M_1 \le 1$$

Binary Deformability and the Radius

$$\tilde{\Lambda} = \frac{16}{13}\frac{(1+12q)\Lambda_1 + q^4(12+q)\Lambda_2}{(1+q)^5} \simeq \frac{16a}{13}\left(\frac{R_{1.4}c^2}{G\mathcal{M}}\right)^6 \frac{q^{8/5}(12-11q+12q^2)}{(1+q)^{26/5}}.$$

This is very insensitive to q for $q > 0.5$, so

$$\tilde{\Lambda} \simeq a' \left(\frac{R_{1.4}c}{G\mathcal{M}}\right)^6.$$

For $\mathcal{M} = (1.2 \pm 0.2)\ M_\odot$, $a' = 0.0035 \pm 0.0006$,

$$R_{1.4} = (11.5 \pm 0.3)\frac{\mathcal{M}}{M_\odot}\left(\frac{\tilde{\Lambda}}{800}\right)^{1/6} \mathrm{km}.$$

For GW170817, $\mathcal{M} = 1.186 M_\odot$, $a' = 0.00375 \pm 0.00025$,

$$R_{1.4} = (13.4 \pm 0.1)\left(\frac{\tilde{\Lambda}}{800}\right)^{1/6} \mathrm{km}.$$

Implied $\Lambda_{1.4} - L$

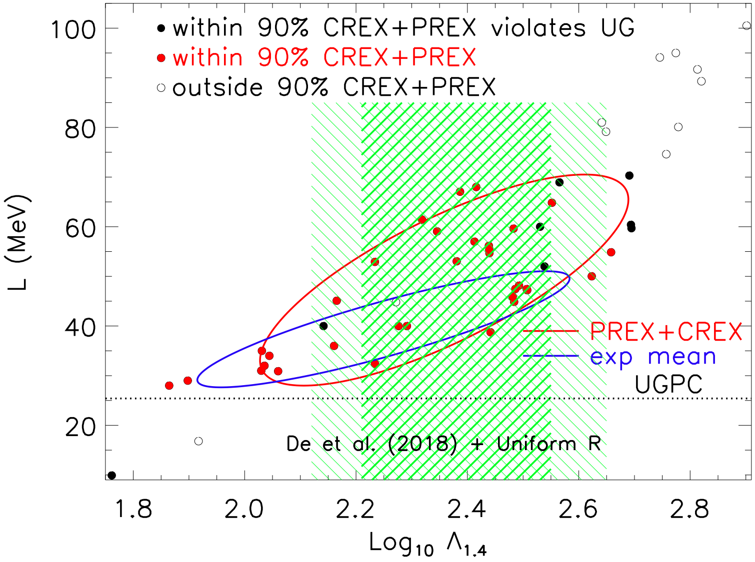

Summary of Astrophysical Observations

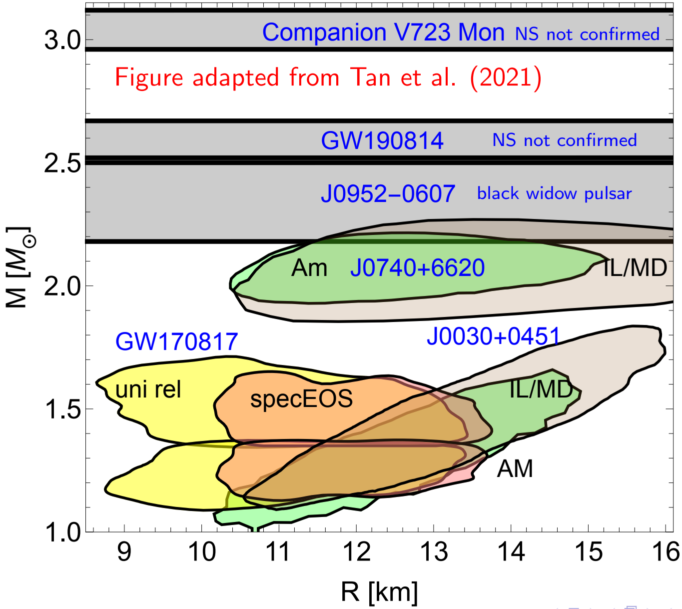

Moment of Inertia

- Spin-orbit coupling is of same magnitude as post-post-Newtonian effects (Barker & O'Connell 1975, Damour & Schaeffer 1988).
- Precession alters orbital inclination angle (observable if system is face-on) and periastron advance (observable if system is edge-on).
- More EOS sensitive than R: $I \propto MR^2$.
- Measurement requires system to be extremely relativistic.
- Double pulsar PSR J0737-3037 is an edge-on candidate; $M_A = 1.338185^{+12}_{-14} M_\odot$.
- Even more relativistic systems are likely to be found, based on faintness and nearness of PSR J0737-3037.

Recent Moment of Inertia Measurement

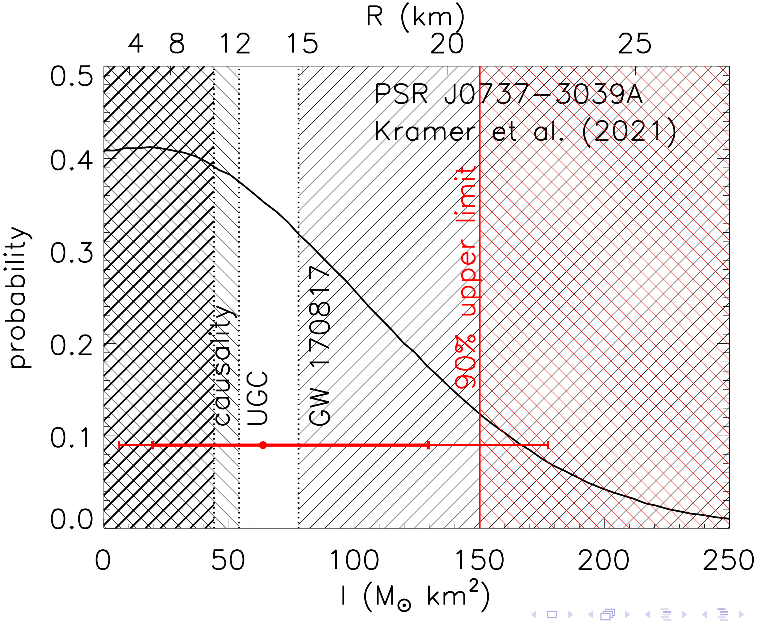

The Urca Processes

Gamow & Schönberg proposed the direct Urca process: nucleons at the top of the Fermi sea beta decay.

$n \to p + e^- + \nu_e$,
$p \to n + e^+ + \bar{\nu}_e$

Energy conservation guaranteed by beta equilibrium

$\mu_n - \mu_p = \mu_e$

Momentum conservation requires $|k_{Fn}| \le |k_{Fp}| + |k_{Fe}|$.

Charge neutrality requires $k_{Fp} = k_{Fe}$, therefore $|k_{Fp}| \ge 2|k_{Fn}|$.

Degeneracy implies $n_i \propto k_{Fi}^3$, thus $x \ge x_{DU} = 1/9$.

With muons $(n > 2n_s), x_{DU} = \frac{2}{2+(1+2^{1/3})^3} \simeq 0.148$

If $x < x_{DU}$, bystander nucleons needed: modified Urca process.

$(n,p) + n \to (n,p) + p + e^- + \nu_e$,
$(n,p) + p \to (n,p) + n + e^+ + \bar{\nu}_e$

Neutrino emissivities:

$\dot{\epsilon}_{MU} \simeq (T/\mu_n)^2 \, \dot{\epsilon}_{DU} \sim 10^{-6} \dot{\epsilon}_{DU}$.

Beta equilibrium composition:

$$x_\beta \simeq (3\pi^2 n)^{-1} (4E_{sym}/\hbar c)^3 \simeq 0.04 \, (n/n_s)^{0.5-2} \ .$$

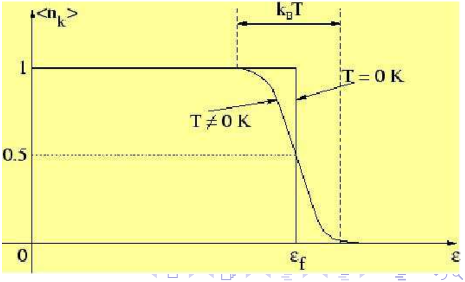

Neutron Star Cooling

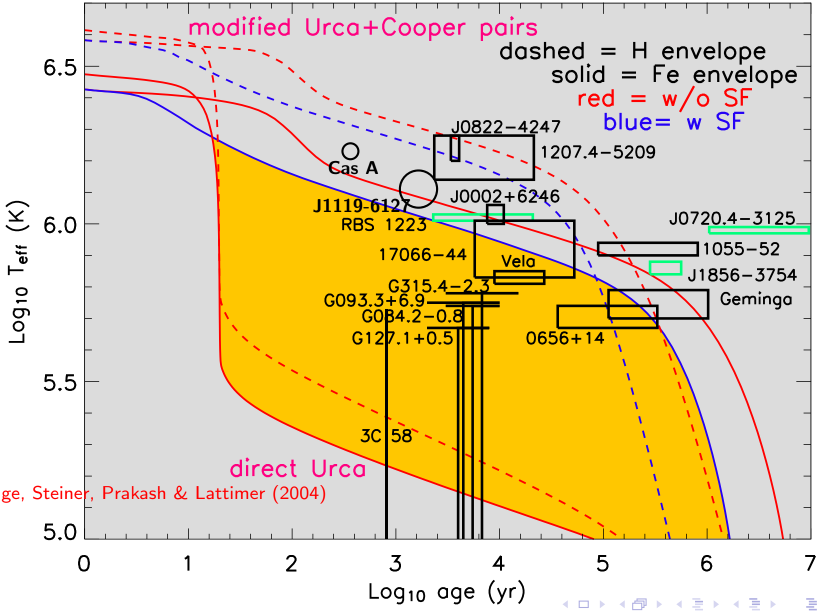

Transitory Rapid Cooling

MU emissivity: $\dot{\varepsilon}_{MU} \propto T^8$

PBF emissivity ($f \sim 10$):
$\dot{\varepsilon}_{PBF} \propto F(T)\ T^7 \propto T^8 \simeq f\dot{\varepsilon}_{MU}$

Specific heat: $C_V \propto T$

Neutrino dominated cooling:
$C_V dT/dt = -L_\nu$

$\implies T \propto (t/\tau)^{-1/6}$
$\tau_{PBF} = \tau_{MU}/f$

$(d\ln T/d\ln t)_{transitory}$
$\simeq (1-10)(d\ln T/d\ln t)_{MU}$
$\simeq (1-25)(d\ln T/d\ln t)_{MU}$ (p SC)

Very sensitive to n $^1S_0$ critical temperature (T_C) and existence of proton superconductivity

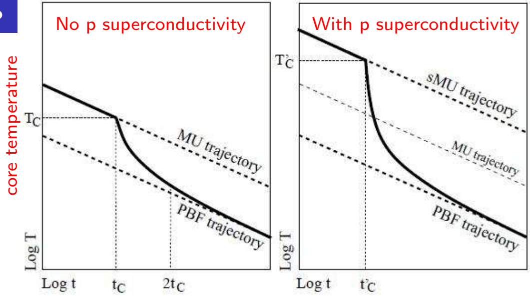

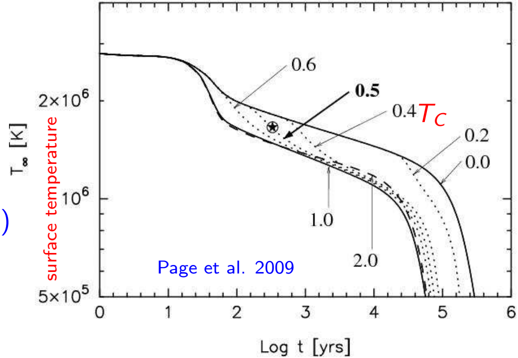

Cas A

Remnant of Type IIb (gravitational collapse, no H envelope) SN in 1680 (Flamsteed).

3.4 kpc distance

3.1 pc diameter

Strongest radio source outside solar system, discovered in 1947.

X-ray source detected (Aerobee flight, 1965)

X-ray point source detected (Chandra, 1999)

1 of 2 known CO-rich SNR (massive progenitor and neutron star?)

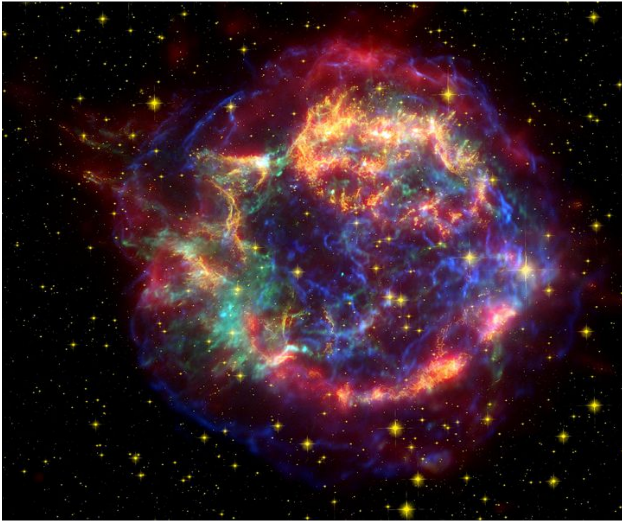

Spitzer, Hubble, Chandra

Cas A Superfluidity

X-ray spectrum indicates thin C atmosphere, $T_e \sim 1.7 \times 10^8$ K (Ho & Heinke 2009)

10 years of X-ray data show cooling at the rate $\frac{d \ln T_e}{d \ln t} = -1.23 \pm 0.14$ (Heinke & Ho 2010)

Modified Urca: $\left(\frac{d \ln T_e}{d \ln t}\right)_{MU} \simeq -0.08$

We infer that
$T_C \simeq 5 \pm 1 \times 10^8$ K
$T_C \propto (t_C L/C_V)^{-1/6}$

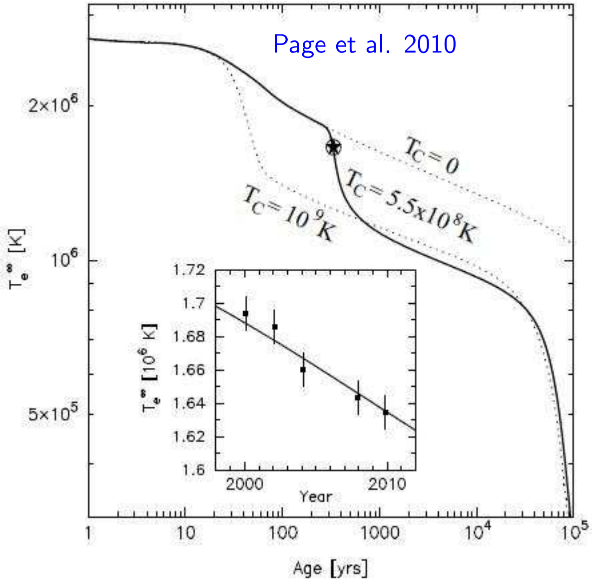

Conclusions

- Nuclear experiments set reasonably tight constraints on symmetry energy parameters and the symmetry energy behavior near the nuclear saturation density.
- Theoretical calculations of pure neutron matter predict very similar symmetry constraints.
- These constraints predict neutron star radii in the range 12 ± 0.7 km.
- Combined astronomical observations of photospheric radius expansion X-ray bursts and quiescent sources in globular clusters suggest $R < 13$ km.
- The nearby isolated neutron star RX J1856-3754 appears to have a radius near 12 km, assuming a C best-fit atmosphere.
- The observation of a 1.97 $M_\odot$ neutron star, together with the radius constraints, implies the EOS above the saturation density is relatively stiff.